




RESEARCH ARTICLE

 OPEN ACCESS 

Follistatin like-1 (*Fstl1*) regulates adipose tissue development in zebrafish

Lucía Guggeri^a, Ileana Sosa-Redaelli^a, Magdalena Cárdenas-Rodríguez^a, Martina Alonso^a, Gisell González^b, Hugo Naya^{c,d}, Victoria Prieto-Echagüe^a, Paola Lepanto^a, and Jose L. Badano ^a

^aHuman Molecular Genetics Laboratory, Institut Pasteur de Montevideo, Montevideo, Uruguay; ^bZebrafish Laboratory, Institut Pasteur de Montevideo, Montevideo, Uruguay; ^cBioinformatics Unit, Institut Pasteur de Montevideo, Montevideo, Uruguay; ^dFacultad de Agronomía, Universidad de la República, Montevideo, Uruguay

ABSTRACT

Obesity is a highly prevalent disorder with complex aetiology. Therefore, studying its associated cellular and molecular pathways may be aided by analysing genetic tractable diseases. In this context, the study of ciliopathies such as Bardet–Biedl syndrome has highlighted the relevance of primary cilia in obesity, both in the central nervous system and peripheral tissues. Based on our previous *in vitro* results supporting the role of a novel Bbs4–cilia–Fstl1 axis in adipocyte differentiation, we evaluated the *in vivo* relevance of the zebrafish orthologous genes *fstl1a* and *fstl1b* in primary cilia and adipose tissue development. Using a combination of knockdowns and a new *fstl1a* mutant line, we show that *fstl1a* promotes primary cilia formation in early embryos and participates in adipose tissue formation in larvae. We also show that *fstl1b* partially compensates for the loss of *fstl1a*. Moreover, in high fat diet, *fstl1a* depletion affects the expression of differentiation and mature adipocyte markers. These results agree with our previous *in vitro* data and provide further support for the role of FSTL1 as a regulator of adipose tissue formation. Dissecting the exact biological role of proteins such as FSTL1 will likely contribute to understand obesity onset and presentation.

ARTICLE HISTORY

Received 14 September 2024
Revised 22 November 2024
Accepted 25 November 2024

KEYWORDS

Adipose tissue; cilia; zebrafish; Bardet–Biedl syndrome; follistatin-like 1


Introduction

Obesity is a major public health issue often leading to several metabolic conditions such as diabetes, hypertension and atherosclerosis [1]. It is a complex disorder both phenotypically as well as at an aetiological level since multiple genes and environmental factors can contribute to disease onset and presentation [2]. In this context, characterizing genetically tractable conditions presenting with obesity is a powerful tool to dissect relevant molecular/cellular components and pathways. Ciliopathies are human diseases caused to different extents by defects in the formation or function of cilia. In agreement with this, several clinical manifestations that include, for example, cystic kidney disease, polydactyly, retinal degeneration, developmental delay, and left–right asymmetry defects among others, are present in different ciliopathies [3–6]. Obesity is primarily present in two of such conditions: Alström (ALMS; OMIM 203,800) and Bardet–Biedl syndrome (BBS; OMIM 209,900).

Primary cilia are complex organelles with a main function in signalling, acting as cellular antennae sensing and transducing both chemical and mechanical

cues [7–9]. In addition to their complex biological function, they are present in most cell types in mammals [10]. Thus, the contribution of primary cilia dysfunction to a given phenotype could involve different signalling pathways and multiple cell types, tissues, and organs. The development of obesity in the ciliopathies highlights this complexity. Cilia in proopiomelanocortin (POMC) and agouti-related protein (AGRP) neurons in the hypothalamus are critical for sensing and integrating different feeding/satiety signalling pathways (reviewed in [11]). As mentioned, one ciliopathy presenting obesity is BBS and BBS proteins play a role in cilia maintenance and function (reviewed in [12]). Furthermore, BBS proteins mediate the localization to the primary cilium of different G protein-coupled receptors (GPCRs) and other components of signalling pathways involved in the regulation of satiety by hypothalamic neurons such as somatostatin receptor type 3 (Sstr3), melanin-concentrating hormone receptor 1 (Mhcr1), neuropeptide Y receptor (NPY2R) and leptin receptor (LepR) [13–16]. Furthermore, BBS proteins also regulate the localization of receptors to the plasma membrane, including LepR [17] and serotonin

CONTACT Paola Lepanto  plepanto@pasteur.edu.uy; Jose L. Badano  jbadano@pasteur.edu.uy  Human Molecular Genetics Laboratory, Institut Pasteur de Montevideo, Mataojo 2020, Montevideo 11400, Uruguay

 Supplemental data for this article can be accessed online at <https://doi.org/10.1080/21623945.2024.2435862>

© 2024 The Author(s). Published by Informa UK Limited, trading as Taylor & Francis Group.

This is an Open Access article distributed under the terms of the Creative Commons Attribution-NonCommercial License (<http://creativecommons.org/licenses/by-nc/4.0/>), which permits unrestricted non-commercial use, distribution, and reproduction in any medium, provided the original work is properly cited. The terms on which this article has been published allow the posting of the Accepted Manuscript in a repository by the author(s) or with their consent.

5-HT_{2C} receptor, a function that is important for the development of obesity in *Bbs1* POMC-specific knockout mice [18]. Targeting different BBS genes in mice recapitulates the obesity phenotype and *Bbs4*^{-/-} animals are characterized by hyperphagia [13,15,16,19–23]. Notably, depletion of BBS proteins in CNS neurons can also lead to obesity due to defects in energy expenditure rather than hyperphagia [24]. Therefore, one main driver of weight gain associated with ciliopathies is thought to be a signalling defect affecting feeding, satiety, and energy expenditure regulation at the level of the CNS.

In addition, different reports underscore an important role for primary cilia and BBS proteins in other relevant organs such as the adipose tissue [11,12,25]. Cilia are required for the commitment of mesenchymal stem cells into the adipocyte lineage [26]. They are also present in preadipocytes and during the beginning of differentiation, being reabsorbed later on [27–30]. Interestingly, the expression of BBS genes follows a similar pattern with high levels of expression in preadipocytes and a significant downregulation once differentiation is ongoing [30,31]. Moreover, depletion of different BBS proteins in preadipocyte cell lines and *in vivo* in mice has been shown to affect adipogenesis [29,32,33]. However, the exact role of BBS proteins in this process and their role on adipose tissue physiology is still poorly understood.

Evaluating the role of cilia and BBS proteins in adipose tissue is therefore critical to understand the development of obesity in ciliopathies as well as non-syndromic obesity. We have shown previously that both cilia and BBS proteins, particularly BBS4, regulate the expression and secretion of Follistatin-like 1 (FSTL1) [30], a secreted glycoprotein that has been implicated in several physiological and pathological processes [34] and initially considered a pre-adipocyte marker since its levels are markedly reduced during differentiation [35]. FSTL1 expression correlates with both the pattern of expression of BBS genes and the presence/absence of cilia [30,35]. Importantly, we showed that both phases of FSTL1 expression are required for adipocyte differentiation in murine 3T3L1 cells: differentiation was inhibited by depleting FSTL1 at the beginning of the process via siRNA but also by supplementing with recombinant FSTL1 to artificially maintain high levels of FSTL1 once differentiation starts. Interestingly, our results also showed that this effect is likely mediated, at least in part, by a novel role of FSTL1 regulating primary cilia formation: depletion of FSTL1 resulted in shortened cilia in both hTERT-RPE and 3T3L1 cells while supplementing with recombinant FSTL1 during 3T3L1 differentiation

inhibited normal cilia reabsorption. Altogether, our results suggested the existence of a BBS4-cilia-Fstl1 axis with a positive feedback loop where cilia regulate FSTL1 expression and secreted FSTL1 regulates cilia formation [30]. Therefore, our data supported an important role for FSTL1 during adipocyte differentiation in cell lines, downstream of BBS4. More recently, FSTL1 depletion was shown to inhibit differentiation to adipocytes of murine embryonic fibroblasts and stromal vascular fraction cells [36].

In this work, we aimed to test the physiological relevance of our findings in cell culture by assessing whether FSTL1 regulates cilia and whether it participates in adipose tissue development *in vivo*. Deleting *Fstl1* in mice results in early postnatal death due to lung development defects [37]. Here, using transient knock-downs and a novel mutant line in *Danio rerio* (zebrafish), we confirmed a role for FSTL1 in cilia length regulation, and we showed that lack of *fstl1* impairs adipose tissue expansion, thus underscoring a novel role for FSTL1 in adipose tissue development.

Results

Knockdown of *fstl1a* and *fstl1b* affect primary cilia formation in zebrafish embryos

Two orthologous genes of mammalian *FSTL1* are present in zebrafish: *fstl1a* (NM_001017860) and *fstl1b* (NM_001039621), located on chromosomes 1 and 9, respectively (Figure S1A-B). Comparison of human FSTL1, mouse *Fstl1*, and zebrafish *fstl1a* and *fstl1b*, showed a high level of homology (Figure S1C-D): in all cases the protein is composed of a signal peptide, followed by an acidic region with no affinity for calcium, a follistatin domain, which is divided into a follistatin-like domain (FOLN) and a Kazal like serine protease inhibitor domain, a calcium-binding EF hand domain and a C-terminal domain with homology to von Willebrand factor type C-like (VWC) [38].

fstl1a and *fstl1b* are expressed during the early development of zebrafish embryos, and previous analyses using morpholinos have shown the participation of these genes in dorso-ventral axis formation [39,40]. We first analysed whether *fstl1a/b* depletion affected cilia formation. We designed splice-blocking morpholinos (MO*fstl1a* and MO*fstl1b*) targeting each gene's exon 2 - intron 2 junctions (Figure 1a). Binding of the MO was predicted to trigger the retention of intron 2 and to introduce a premature stop codon in both cases. To assess each morpholino's targeting efficiency, we performed RT-PCR using mRNA from control and morphant embryos. Amplification from wild-type

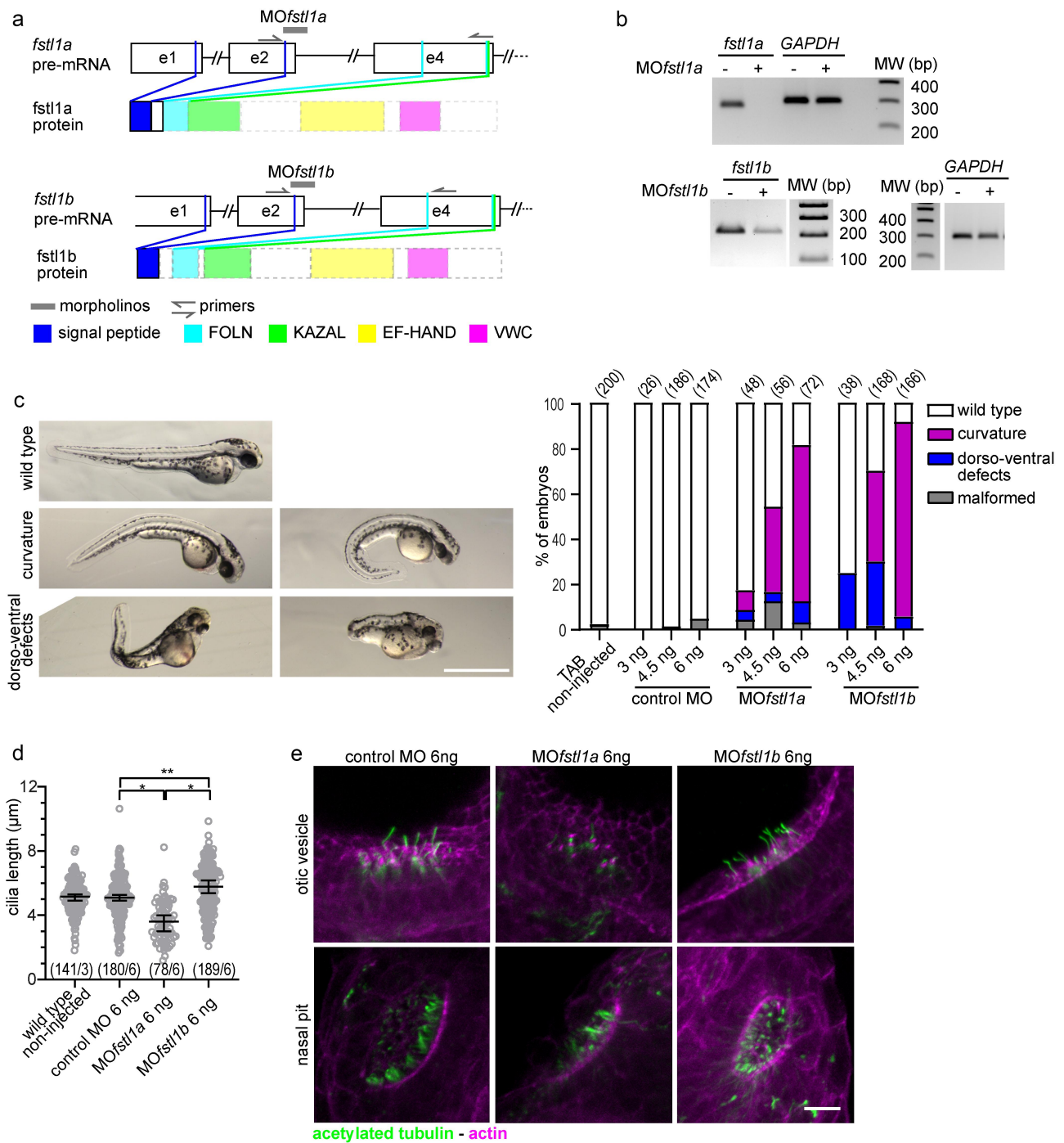


Figure 1. *fstl1a* and *fstl1b* knockdown affect primary cilia formation in early embryos.

a) Diagram depicting the partial genomic structure of *fstl1a* and *fstl1b* to show the site of morpholino binding (grey bar) to mRNA and the location of primers (arrows) used to evaluate knockdown efficiency. Also, schematic representations of the corresponding protein structures are shown. b) Gel image showing RT-PCR results demonstrating impaired amplification of *fstl1a* and *fstl1b* in the MO*fstl1a* and MO*fstl1b* morphant embryos, respectively. *Gapdh* was used as control. c) Low magnification images of 48 hpf wild-type and morphant embryos, and graphs showing the distribution of embryos in distinct phenotypic classes according to severity at the morpholino doses tested. The pooled data from three experiments are presented; the number of embryos analysed in each condition is indicated within brackets. d) Dot plot with the quantification of ciliary length in Kupffer vesicle of 12 somite-stage control and morphant embryos. The pooled data from a single experiment are presented; the total number of cilia measured/number of embryos is indicated in brackets. Plot: individual cilia length values and median \pm CI (95%) (* $p < 0.0001$; (** $p = 0.0019$; Games–Howell test). e) Representative images showing primary cilia (evidenced through acetylated tubulin immunostaining) in the nasal pit and otic vesicle of 48 hpf embryos injected with either 6 ng of control MO, MO*fstl1a* or MO*fstl1b*. Phalloidin staining of F-actin was used to delineate the organ. Scale bars: C: 1 mm; E: 10 μ m.

mRNA resulted in PCR amplicons of 282 bp and 212 bp for *fstl1a* and *fstl1b*, respectively, whereas the aberrantly spliced mRNA was not expected to yield a PCR product due to the size of the retained intron (>10 kb and >60 kb for *fstl1a* and *fstl1b* respectively). Our results show that the MOs efficiently affected the splicing of both *fstl1a* and *fstl1b* (Figure 1b).

We analysed the external phenotype of 48 hpf embryos injected with different doses of MO*fstl1a* and MO*fstl1b*. Knockdown of each gene individually resulted in defective ventral curvature and smaller eyes (Figure 1c). We also observed embryos with a significant shortening of the body axis and varying degrees of defects in the formation of the tailbud, indicating defects in dorsal-ventral axis formation. Previous work on *fstl1a* and *fstl1b* indicated a role for these genes in blocking ventral fates in combination with other bone morphogenetic proteins (BMPs) agonists [40]. Of note, embryos with dorso-ventral defects appeared with higher frequency after injection of MO*fstl1b*, consistent with the more prominent role reported for this gene in dorso-ventral patterning ([39,40]; Figure 1c).

Next, we analysed cilia in Kupffer's vesicle (KV), a ciliated transient embryonic structure involved in left-right patterning [41]. We performed immunostaining using antibodies against acetylated tubulin and assessed cilia using confocal microscopy (Figure S2). Knockdown of *fstl1a* using a full dose of morpholino (6 ng) resulted in a significant shortening of cilia: cilia in un-injected embryos and embryos injected with control morpholinos were $5.1 \pm 1.1 \mu\text{m}$ (mean \pm SD) and $5.1 \pm 1.4 \mu\text{m}$ long, respectively, whereas cilia in *fstl1a* morphants measured $3.6 \pm 1.3 \mu\text{m}$ (Figure 1d). In contrast, cilia in embryos injected with MO*fstl1b* were $5.6 \pm 1.5 \mu\text{m}$ long. Therefore, while knockdown of *fstl1a* inhibited cilia formation, *fstl1b* knockdown resulted in elongated cilia in KV (Figure 1d). In agreement with that, only *fstl1a* morphants presented a clear cilia phenotype in the otic vesicle and nasal pit, two heavily ciliated structures (Figure 1e). These results showed that while *fstl1a* and *fstl1b* play a role in cilia length regulation, their depletion results in opposing phenotypes. Of note, the effect of *fstl1a* depletion on cilia entirely agrees with our previous report in cells [30].

Generation of a *fstl1a* KO zebrafish line

Next, we sought to assess the role of *fstl1* in adipose tissue development. Given the transient effect of morpholinos and that fat depots start developing in the larval stage (beginning at 10 days post-fertilization), we used CRISPR-Cas9 to generate a novel *fstl1* mutant

line. Based on the previous results showing a pro-ciliogenic role for *fstl1a* we selected this gene to continue our work and designed two guide RNAs (gRNA1 and gRNA2) targeting exon 3 (Figure 2a). We tested their editing efficiency by co-injecting one-cell embryos with Cas9 mRNA and each gRNA, individually and in combination. The injected embryos showed abnormal external phenotypes at 48hpf, including shortening of the body axis with tailbud malformation and dorsal curvature, reminiscent of the dorso-ventral axis defects observed in morphant embryos (Figure 2b). gRNA1 generated a higher percentage of embryos with dorso-ventral phenotype than gRNA2 and a similar percentage of embryos with severe defects. Injection of the combination of both gRNAs gave similar results to gRNA1 injection (Figure 2c). We analysed the genomic region encompassing the target site in *fstl1a* by PCR amplification using primers flanking exon 3 in embryos injected with gRNA1 (Figure 2a). Initial heteroduplex analyses of individual embryos indicated the presence of mutations in the targeted region (Figure 2d). Thus, we selected gRNA1 to generate the KO line.

Since mutations on *fstl1a* produced morphological alterations that could be incompatible with later development, we chose to generate the mutant line using Cas9-nanos mRNA, therefore restricting Cas9 expression to the germ line of injected embryos. Thus, we minimized the mutation of *fstl1a* in somatic cells, which could affect the development of founder adult fish [42]. We then bred the injected embryos to adulthood and out-crossed them with wild-type fish to evaluate the *fstl1a* mutations that were segregated into the progeny. The embryos obtained were used to amplify and sequence the region surrounding the PAM motif, where we identified several indels, many of which resulted in frameshifts and premature termination codons (PTCs) (Figure 2e). We selected a 1 bp insertion (adenine nucleotide) that interrupts a Cys codon at position 40 (TGT) and generates a PTC (TAG) (outlined in Figure 2e). We outcrossed the parental fish bearing this mutation with wild-type fish for an additional generation to isolate the desired mutation and minimize possible off-target effects. As mentioned, the selected mutation introduces a PTC early in the coding sequence, and thus no functional *fstl1a* protein was expected in homozygous mutant fish. Moreover, the mutant transcript was expected to be degraded at the mRNA level by non-sense mediated decay (NMD), therefore resulting in a reduction of *fstl1a* mRNA levels. We evaluated larvae derived from in-crosses of the third generation through qPCR and as expected, we observed a significant reduction of *fstl1a* mRNA levels

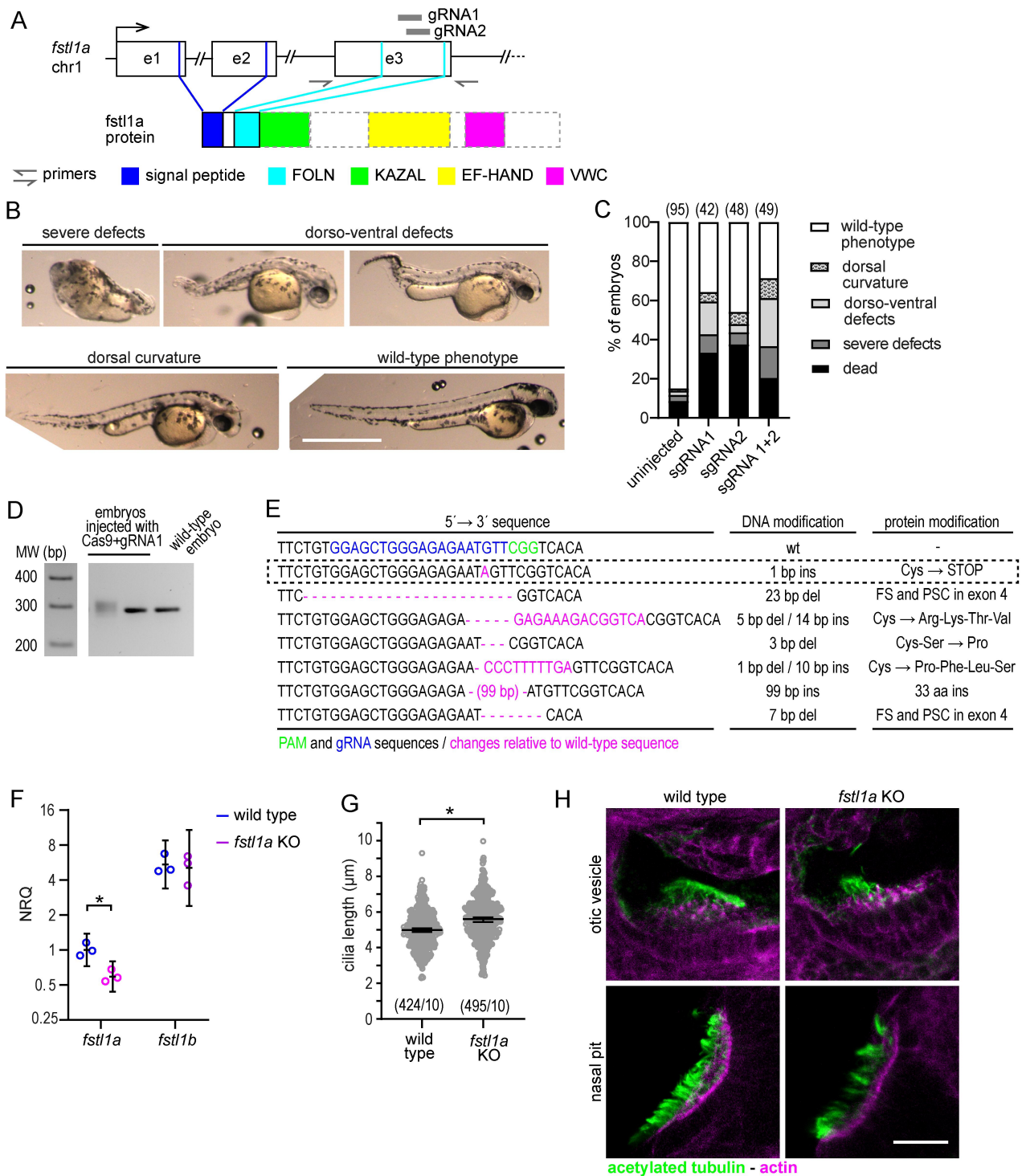


Figure 2. Generation of a *fstl1a* KO line.

a) Diagram depicting the partial genomic structure of *fstl1a* showing the recognition site of gRNAs at exon 3 (grey bars) and of the generic primers used (arrows) for heteroduplex analysis and sequencing of the region. b) Low magnification images of embryos injected with *fstl1a* gRNA 1 and 2 showing examples of the distinct phenotypic classes. c) Plot of the percentage of embryos in each of the following phenotypic classes: wild type, dorsal curvature, dorso-ventral defects, severe defects, dead. Data from a single experiment; the total number of embryos is indicated in brackets. d) Gel image showing the amplification (by PCR) of the region flanking the PAM sequence using the generic primers mentioned in (a) from wild-type and Cas9 + gRNA1 injected embryos. e) Sequence alignments of the different mutations found in embryos derived from the cross of F0 individuals and wild types. The dashed rectangle indicates the allele selected for further work. bp: base pairs; ins: insertion; del: deletion; FS: frame shift; PSC: premature stop codon. f) Dot plot showing qPCR results for *fstl1a* and *fstl1b* in pooled wild-type and *fstl1a* KO 48hpf embryos from the third generation. Plot: technical replicates and mean \pm CI (95%); NRQ: normalized relative quantity; (*) $p = 0,007$, t-test. g) Dot plot showing the quantification of the length of primary cilia in Kupffer's vesicle of

(approximately 40%) in 48hpf embryos of the knockout (KO) line (Figure 2f). Notably, *fstl1b* mRNA levels were not affected in *fstl1a* mutants (Figure 2f).

We then evaluated the external phenotype and primary cilia length, in KV, otic vesicle and nasal pit in wild-type and *fstl1a* KO homozygous embryos derived from the F3 generation (Figure 2g,h). Mutant embryos did not present evident external phenotypes (not shown) or significant cilia defects in the otic vesicle and nasal pit at 48hpf (Figure 2h), although we cannot discard subtle effects on cilia length and number. Unexpectedly, our results did show a small but statistically significant increase in KV's primary cilia length in *fstl1a* KO ($5.6 \pm 1.2 \mu\text{m}$) compared to wild-type embryos ($5.0 \pm 1.0 \mu\text{m}$) (Figure 2g). In sum, we generated a *fstl1a* knockout fish line, without appreciable morphological alterations in early embryonic stages.

Depletion of *fstl1a* affects adipose tissue formation

Next, we analysed *fstl1a* mutant larvae to evaluate adipose tissue. Since there were no previous studies of the expression of *fstl1a* or *fstl1b* in zebrafish larvae, we first performed qPCRs for both genes using RNA from the isolated fat of 21 and 28 dpf wild-type larvae. *fstl1b* showed higher expression than *fstl1a* in all the conditions tested (Figure 3a). As expected, *fstl1a* mRNA levels were reduced in our mutant line: KO larvae of 21 dpf showed an 80% reduction in the expression of *fstl1a* compared to wild types. Again, the effect was specific since *fstl1b* levels were unaffected (Figure 3b).

To analyse adipose tissue formation, we grew wild type and *fstl1a* KO larvae in regular diet until 15 dpf, we then separated them in two groups and grew them in two different feeding schemes: standard and high-fat diet (HFD) (Figure 3c). At 21 dpf, we labelled them with the lipophilic vital dye Nile Red and acquired transmitted light and fluorescence images to measure the developmental stage and the area of adipose tissue as previously reported [43,44] (Figure 3d). While a standard diet allowed us to evaluate the basal ability of the tissue to expand, an HFD diet would provide information about the tissue's response to increased energy availability. The pooled results of three independent experiments (Figure S3A) comparing wild-type and *fstl1a* KO larvae are presented in Figure 3e. The

area of the adipose tissue depends on the developmental stage of larvae (measured as the standard length, SL) through a non-linear relationship [45]. Thus, we used a linear mixed model fit on the square root-transformed area data to analyse the possible differences among conditions. We set SL as a covariate, genotype, and diet as fixed effects, and experiment as an aleatory factor (Figure S3). Using this model, we could explain 89% of the variance in the square root of the area, with residuals normally distributed, indicating an acceptable fit (Figure S3C and S3D). As expected, the developmental stage (SL) was a main variable affecting positively the adipose tissue area. Diet was the second most important factor, with high-fat diet inducing an increase in the square root of the adipose tissue area compared to the standard diet (Figure S3B, S3E and S3F). Notably, the analysis indicated that genotype was also an important factor: the *fstl1a* KO genotype decreased the square root of adipose tissue area compared to the wild-type genotype in both diets (Figure S3B and S3G). Importantly, the difference in adipose area between mutant and control larvae was also significant when we analysed each diet individually (Figure 3e). Despite observing a trend towards a more pronounced phenotype in HFD, the effect of the genotype in each diet was not significantly different (not shown). Thus, our results indicate that depletion of *fstl1a* impairs adipose tissue formation.

fstl1a depletion is partially compensated by *fstl1b*

As mentioned, *fstl1a* morphants showed shortened primary cilia at early embryonic stages and evident external defects, phenotypes that were not completely recapitulated in the *fstl1a* KOs. Thus, we reasoned that compensatory mechanisms may be acting in the KO line. Given the high homology and similar pattern of expression between the two paralogs ([39]; Figures 2f, 3a), one possibility was that *fstl1b* could compensate for the depletion of *fstl1a*. To test this, we injected control and *fstl1b* morpholinos into wild-type and *fstl1a* KO embryos and measured primary cilia length in KV. Primary cilia were shorter in *fstl1a* KO embryos injected with a full dose (6 ng) of *fstl1b* morpholino ($4.7 \pm 1.3 \mu\text{m}$) compared with wild-type embryos injected with *fstl1b* morpholino ($6.1 \pm$

12 somite-stage wild type and *fstl1a* mutant embryos. The pooled data from a single experiment are presented; the total number of cilia measured/number of embryos is indicated in brackets. Plot: individual length values and median \pm CI (95%). (*) $p = 3.8 \times 10^{-14}$, Mann-Whitney test. h) Representative immunofluorescence images showing primary cilia (acetylated tubulin) in the nasal pit and otic vesicle of 48 hpf wild-type and *fstl1a* KO embryos. Scale bars: B: 1 mm; H: 20 μm .

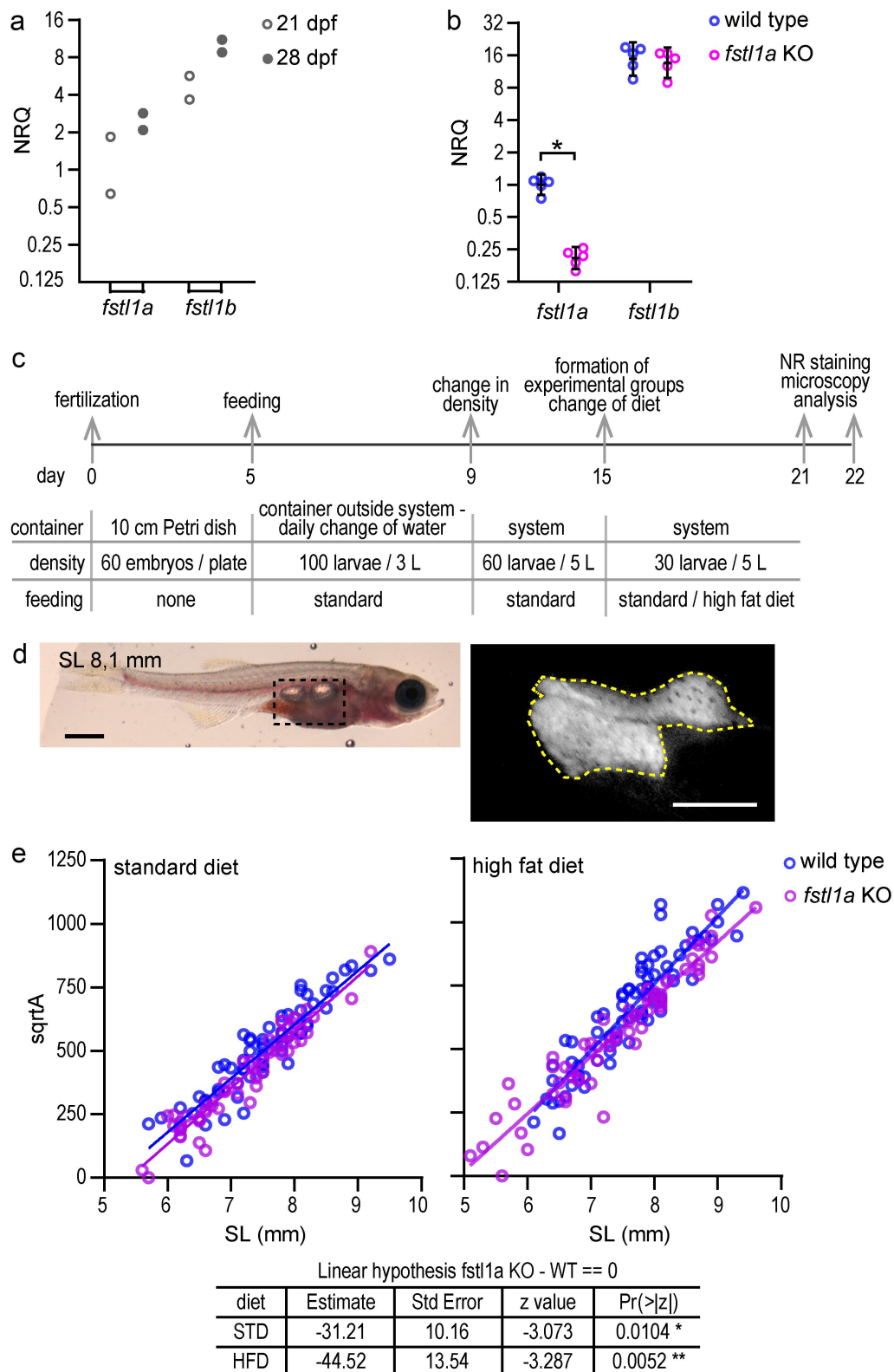


Figure 3. *fst1a* KO larvae have less adipose tissue than wild-type larvae.

a) Dot plot showing the qPCR results to assess the levels of expression of *fst1a* and *fst1b* in the isolated abdominal fat deposit of 21 and 28 dpf wild-type larvae (the mean *fst1a* level at 21 dpf was used as reference; samples from two larvae). b) Dot plot showing the qPCR results for *fst1a* and *fst1b* in the abdominal region of 21 dpf wild-type and *fst1a* KO larvae. Five larvae were analyzed in each condition. Plot: individual NRQ values and mean \pm CI (95%). (*) $p = 0.012$, Mann-Whitney test. c) Schematic representation of the protocol followed to perform the diet experiments. d) Examples of the panoramic bright field and epifluorescence images of Nile Red stained larvae used to quantify the standard length (SL) and extension (area) of adipose tissue. Scale bar: 1 mm (left image); 0.5 mm (right image). e) Dot plots comparing the square root of the area of the adipose tissue vs SL of wild-type and *fst1a* KO larvae in standard and high-fat diets. The straight lines are the least squares fit to the pooled data from three experiments. The statistical comparison was made using a linear mixed model fit and Tukey contrasts (bottom table) (see the complete analysis in Figure S3).

1.6 μm) or with *fstl1a* KO embryos injected with control morpholino (5.6 \pm 1.4 μm) (Figure 4a). In contrast, a sub-dosis of *fstl1b* morpholino (4.5 ng) had no effect on cilia length. These results indicate that *fstl1b* partially compensates for the cilia-associated function of *fstl1a* in the KO line. To test whether this

compensatory function was also occurring during the formation of adipose tissue, we generated an F0 crispant for *fstl1b* in the *fstl1a* KO background. We generated RNPs of four guide RNAs directed to *fstl1b* with Cas9 protein and injected different amounts in one-cell *fstl1a* KO embryos. Since our aim was to evaluate

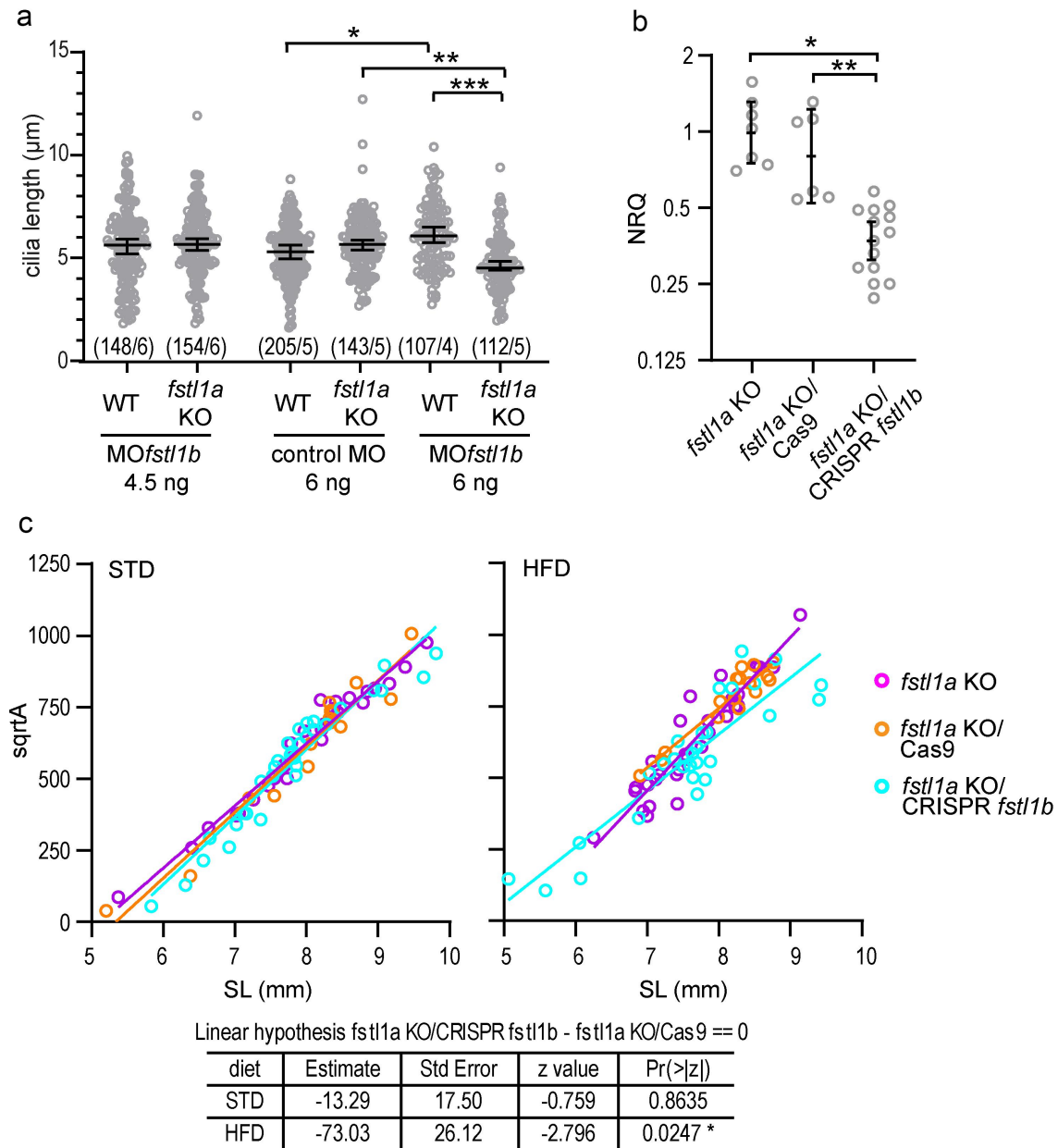


Figure 4. *fstl1b* compensates *fstl1a* depletion.

a) Dot blot with the analysis of cilia length in Kupffer's Vesicle of wild-type or *fstl1a* KO embryos injected with different doses of control or *fstl1b* morpholino. The pooled data from a single experiment is presented; the total number of cilia measured/number of embryos is indicated in brackets. Plot: individual length values and median \pm CI (95%). (*) $p = 1.9 \times 10^{-4}$; (**) $p = 4.2 \times 10^{-7}$; (***) $p = 2.8 \times 10^{-9}$; Mann-Whitney test. b) Dot blot showing the qPCR results assessing the expression level of *fstl1b* mRNA in *fstl1a* KO larvae un-injected (seven larvae analysed), injected with Cas9 protein (six larvae analysed) or crispant for *fstl1b* (14 larvae analysed). Plot: individual NRQ values and mean \pm CI (95%). (*) $p = 8.9 \times 10^{-4}$; (**) $p = 0.0034$; Mann-Whitney test. c) Dot blot showing the comparison of the square root of the adipose tissue area vs SL of *fstl1a* KO larvae un-injected, injected with Cas9 protein or crispant for *fstl1b*, in standard and high-fat diets. The straight lines are least squares fit to the data. The statistical comparison was made using a linear mixed model fit and Tuckey contrasts (bottom table) (see the complete analysis in Figure S3).

adipose tissue formation at 21 dpf, we looked for RNP doses that allowed embryos to develop correctly until that stage with a consistent reduction in *fstl1b* mRNA. Using RNPs at lower doses than the previously reported ones [46] was sufficient to reduce *fstl1b* mRNA levels in crispant larvae to 50% or less than control larvae at 21 dpf (Figure 4b). In this condition, we performed a diet assay as previously detailed (Figure 3c). *fstl1b* crispant larvae in the *fstl1a* KO background significantly reduced adipose tissue area compared to *fstl1a* KO larvae injected with Cas9 protein alone only in HFD (Figure 4c and S3). Thus, our results showed that *fstl1b* can compensate for the absence of *fstl1a* also in the context of adipose tissue formation at least upon challenging zebrafish larvae with HFD.

Changes in differentiation and mature adipocyte markers characterize *fstl1a* KO adipose tissue

To gain insight into the mechanism/s underlying the effect of *fstl1* in adipose tissue expansion, we quantified the expression of marker genes associated with adipose cell differentiation and fat mobilization using qPCR. Although our results indicated that both *fstl1a* and *fstl1b* participate in adipose tissue development in zebrafish larvae, we focused the analysis on the adipose tissue of the *fstl1a* KO line for two reasons: i) *fstl1a* depletion was sufficient to produce a visible reduction in adipose tissue formation and ii) to avoid the variability introduced by *fstl1b* knockdown in F0 crispants. We extracted RNA from the abdominal region of 21 dpf larvae with standard lengths between 7,7 and 8,7 mm and performed qPCR for the different markers.

We first analysed if the genotype and diet affected the expression of the selected genes, performing a two-way ANOVA analysis. This test identified an interaction between diet and genotype for differentiation markers (*pparg1*, *cebpa*) and mature adipocyte markers (*fabp4a*), suggesting that the genotype modifies the effect of the diet on the number of cells going through differentiation and leading to mature adipocytes (Figure 5a, bottom row). Meanwhile, genotype alone affected a different subset of markers (*zfp423*, *pparg1*, *adipoqb*, *pln2* and *fabp4a*; Figure 5a, middle row) compared to diet (*dlk1*, *zfp423*, *pparg1*, *pparg2*, *adipoqb* and *fabp4a*; Figure 5a, top row). Performing a pairwise comparison among groups showed lower expression levels of several genes in *fstl1a* KOs compared to wild types only in HFD, including the preadipocyte marker *zfp423*, differentiation markers *pparg1* and *cebpa*, and the mature adipocyte markers *fabp4a* and *adipoqb* (Figure 5b). We performed the same analysis for some genes associated with fat

mobilization, including *srebfl1*, *cd36*, *lpla*, *dgat2* and *pnpla2* (Figure S4). We found an effect of diet on genes associated with fat accumulation (*srebfl1*, *cd36* and *lpla*), but no significant differences could be detected associated with genotype in the two-way ANOVA or the pairwise comparison (Figure S4). These results suggest that *fstl1a* could play a role during adipocyte differentiation. Consistently, *gli1*, *patched 1* and *patched 2*, all members of the anti-adipogenic Shh signalling pathway [47,48], showed a trend to upregulation with HFD feeding in *fstl1a* KO larvae compared with wild-type larvae (Figure 5b).

Altogether, our data showing the downregulation of differentiation markers *pparg1*, *pparg2* and *cebpa* in the KO-HFD condition compared with wild type-HFD, the alteration in Shh signalling, and the stagnation of mature adipocyte markers *adipoqb* and *fabp4a*, suggest that *fstl1a* could promote differentiation of new adipocytes.

Discussion

Understanding the cellular/molecular basis of the different phenotypes that characterize a ciliopathy, such as BBS, requires dissecting the functional role of BBS-associated genes/proteins in different tissues and organs. The development of obesity is one clear example. While weight gain in BBS patients and animal models is driven by a cilia-based central nervous system defect leading to hyperphagia, different lines of evidence indicate that the final presentation of obesity can be directly influenced by the role of BBS proteins in peripheral tissues (for some examples see [32,33,49,50]). In this context, we previously uncovered a functional interaction between BBS4 and FSTL1 likely relevant to obesity in BBS: we showed that FSTL1 plays a role regulating both cilia length and adipogenesis downstream of BBS4 in 3T3L1 preadipocytes [30]. The role of FSTL1 in adipogenesis has been further supported by other work showing that *Fstl1* KO mouse embryonic fibroblasts are unable to differentiate to adipocytes [36,51]. Here, we expand on these results showing that depletion of *fstl1* in zebrafish affects both cilia and adipose tissue development.

To investigate *fstl1* function, we targeted both zebrafish *fstl1* paralogs (*fstl1a* and *fstl1b*), individually and together, using a combination of morpholinos, F0 CRISPR-Cas9 and a novel *fstl1a* mutant line. One first aspect worth discussing is the different phenotypic outcome between *fstl1a* morphants and the mutant line: while morphant embryos presented phenotypes associated with primary cilia or dorso-ventral axis formation defects, those early embryonic phenotypes were

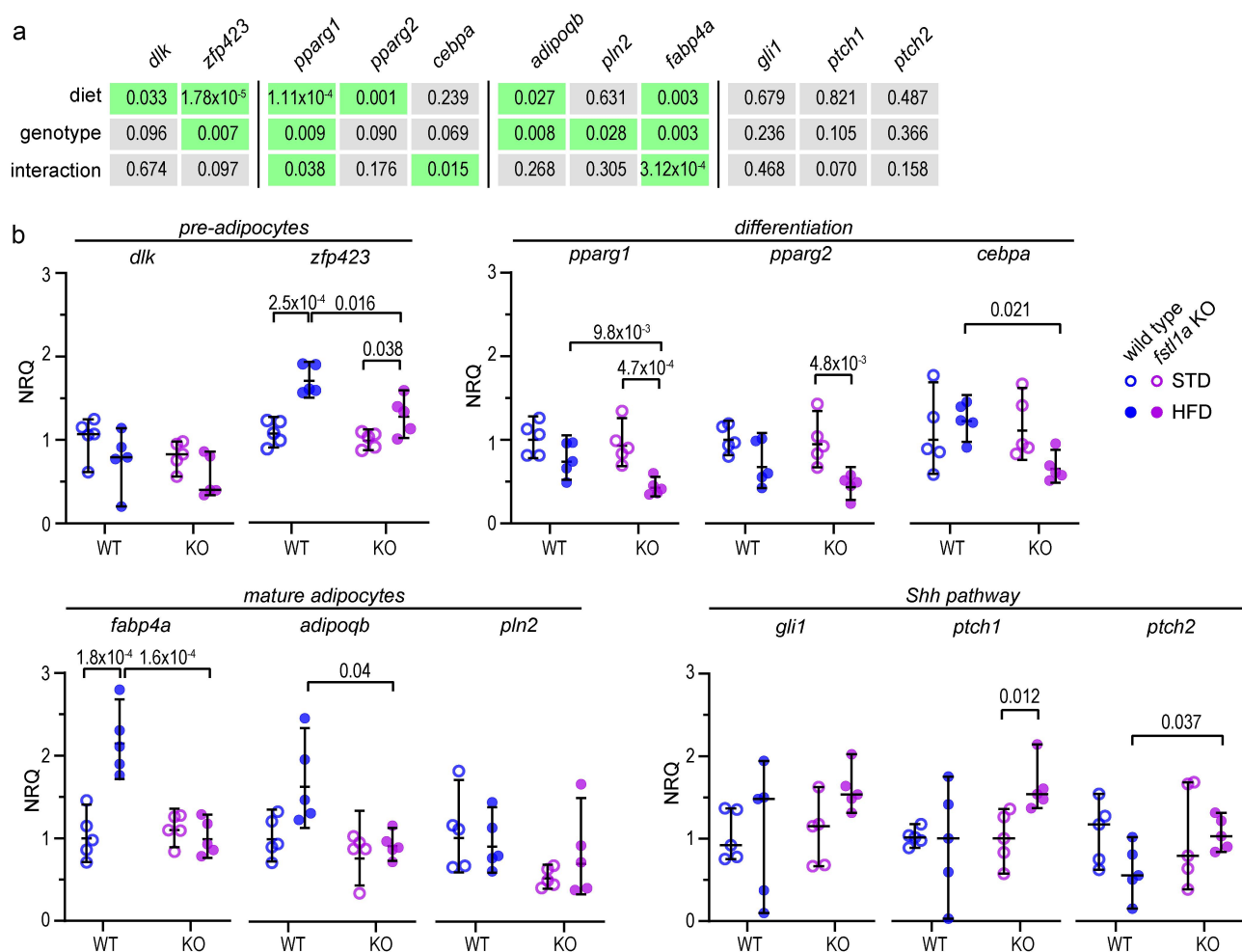


Figure 5. Differentiation and mature adipocyte markers are downregulated in *fstl1a* KO larvae under high fat diet compared to wild types.

a) Table showing the expression analysis for different genes associated with preadipocytes, adipogenesis (differentiation), mature adipocytes, and activation of the Shh signalling pathway. qPCR results were analysed using a two-way ANOVA to evaluate the effect of diet and genotype on the expression of the different genes. The table indicates the p-values of the simple main effect analysis and the interaction between diet and genotype for each gene. b) Dot plots with the individual NRQ values and the mean \pm CI95% of mRNA for different preadipocyte (*dlk1*, *zfp423*), differentiation (*pparg1*, *pparg2*, *cebpa*) and mature adipocyte (*fabp4a*, *adipoqb*, *pln2*) marker genes, as well as genes indicative of Shh pathway activation (*gli1*, *ptch1*, *ptch2*) in the abdominal region of wild-type (WT; blue) or *fstl1a* KO (KO; magenta) larvae under standard (○; empty circle) or high fat diet (●; full circle). Five larvae from one diet experiment were analysed in each condition. Significant pairwise differences are indicated with their p-values (Tuckey post-hoc test).

not observed in the *fstl1a* mutant zebrafish line. Discrepancies between morphants and their respective genomic mutants are well-documented in zebrafish and other animal models, and different mechanisms have been proposed to be involved [52–54]. In some cases, the mutation can trigger changes in splicing, thus bypassing the mutated exon, and producing an alternative isoform that can retain at least partial functionality [55]. However, this is not likely to be a significant phenomenon in our mutant line. The *fstl1a* mutation reported here introduces a PTC in exon 3 and we observed a marked reduction in *fstl1a* mRNA levels by qPCR using primers located at the 3' end of the

mRNA (in exons 6 and 8). This result indicates a significant reduction in *fstl1a* mRNA levels, likely due to NMD rather than the inability to detect *fstl1a* splice isoforms lacking the mutated exon.

Degradation of mutant transcripts by NMD has been shown to trigger the upregulation of related genes through transcriptional adaptation, resulting in compensatory effects [52,56]. As mentioned, *fstl1* is duplicated in the fish (*fstl1a* and *fstl1b*) and the two paralogs show significant similarity at the genomic and protein level, thus making *fstl1b* a strong candidate to underly compensation in the *fstl1a* KO. Our results show that, indeed, *fstl1b* can compensate, at least in part, for the

depletion of *fstl1a*, but this effect does not rely on transcriptional changes: *fstl1b* mRNA levels were not altered in the *fstl1a* mutant fish. Interestingly, compensation is achieved despite the two paralogs having seemingly different functions when targeted individually: depleting *fstl1a* led to shortened cilia in KV while knocking down *fstl1b* produced the opposite effect. However, when we targeted *fstl1b* with morpholinos in the *fstl1a* mutant background we observed cilia shortening. Therefore, while our results support a role for *fstl1b* in cilia length regulation, its specific action in that context appears to be modulated by the presence/absence of *fstl1a*. In other words, in the presence of both paralogs, *fstl1b* appears to inhibit cilia formation, but in the absence of *fstl1a*, *fstl1b* substitutes its function, at least to a certain extent. Additional experiments will be needed to fully understand this functional interplay between *fstl1a* and *fstl1b* in primary cilia formation. Fstl1 is a secreted protein that in mammals has been shown to bind different ligands (such as bone morphogenetic proteins, BMPs) and receptors (e.g. Dip2a) [34,57–59]. Whether those interactors are important in the context of cilia length regulation has yet to be discovered. Still, our previous data showed that it is the secreted FSTL1 that regulates cilia in a non-cell autonomous fashion [30]. One scenario, therefore, is that the two paralogs compete with different affinities for protein interactions relevant to cilia. In addition, FSTL1 has been proposed to be able to form dimers [38]. Thus, functional differences between heterodimers and homodimers could also be involved. Finally, compensation could arise from the activation of functionally related pathways. For example, a genomic mutant of the ciliary protein CEP290 presented upregulation of other cilia-related genes [60]. Comparing morphant and *fstl1* mutants through ‘omic’ approaches, such as RNAseq studies, will likely be required to fully address this possibility and provide mechanistic information to understand the role of Fstl1 in the context of cilia.

FSTL1 is a protein that has been linked to different biological processes involving multiple tissues and cell types. Its complete absence results in neonatal lethality in mice [61] and thus a conditional targeting approach is generally needed to study its function in murine models (for some examples see [62–64]). Regarding adipose tissue, Fang and colleagues have used the *aP2* (*Fabp4*)-Cre line to target *Fstl1* in mature adipocytes [36]. However, the scarcity of suitable Cre-lines has impaired testing the functionality of *Fstl1* during early adipogenesis, an important factor considering our previous results. Zebrafish has become a widely used model in biomedical research and presents strengths

to analyse adipose tissue. From a technical standpoint, the fish allows the assessment of tissue development *in vivo* from early stages, and from a physiological perspective, there are many similarities with adipose tissue in mammals [65]. Contrasting with the lack of phenotypes in early embryos, our results demonstrate that depletion of *fstl1a* hindered adipose tissue development in zebrafish larvae despite a potential compensatory effect exerted by *fstl1b*. Interestingly, it has been speculated, and some initial studies support the possibility, that the degree of compensation can indeed vary at different developmental stages ([66] and references within). Alternatively, being able to observe a phenotype in adipose tissue but not in cilia could depend on the requirement for *fstl1a* and/or the ability of *fstl1b* to compensate in each process.

We observed a defect in adipose tissue expansion regardless of diet: adipose tissue area in *fstl1a* mutant larvae was significantly reduced compared to controls in both standard and high-fat diets. However, the phenotype appeared to be more severe in HFD, albeit no statistically significant interaction between genotype and diet was detected. In the gene marker analysis and the interaction between *fstl1a* and *fstl1b*, significant differences were detected only in HFD. These results suggest that the challenge imposed by HFD on adipose tissue physiology and development might expose more evidently the defects caused by *fstl1a* depletion. Interestingly, a recent study showed that knocking out *Fstl1* specifically in mature adipocytes in mice impairs weight gain only in HFD [36]. Different possibilities could explain the difference in the response to Fstl1 depletion in normal diet between that work and the results presented here. For example, there are important differences in the timing and extent of *fstl1* elimination between the models: a whole-body KO in our work and a mature adipocyte knockout in the murine model. Also, it is possible that our experimental setup, assessing adipose area in a large number of individuals during early developmental stages, had higher sensitivity allowing to document milder phenotypes. Overall, our results show that *fstl1* plays a role during adipose tissue development, but also suggest that its presence and/or its function could become more critical during the response of the tissue to an increase in energy availability. Further studies will be required to fully determine the role of Fstl1 in different nutritional scenarios.

Regarding the mechanism of action of *fstl1a* on adipose tissue expansion, the analysis of molecular markers indicates that part of *fstl1a* function could involve the regulation of adipocyte differentiation, in agreement with our previous results in 3T3L1 murine

cells [30]. Based on different lines of evidence, it is tempting to speculate that it could exert this regulation, at least in part, via its role regulating cilia. Our results from previous *in vitro* experiments [30] and our current *in vivo* data indicate that *Fstl1* can regulate cilia. We documented this role in early embryos, although cilia in *fstl1a* mutants were not severely affected due to compensation by *fstl1b*. As discussed, it is possible that compensation is not taking place at the larvae stages in which we analyse adipose tissue. Unfortunately, we were not able to directly assess cilia in adipose tissue of larvae due to technical difficulties. Having said that, not observing a structural phenotype such as a cilia length defect would not necessarily mean that the organelle is fully functional. Importantly, cilia are needed during adipogenesis both mediating pro-adipogenic, such as IGF-1 [67], and anti-adipogenic signals, such as *Shh*, a pathway that heavily relies on the cilium as a signalling platform [68–71]. Interestingly, we observed an upregulation of *Shh* genes in *fstl1a* KO fish in HFD suggesting misregulation of the pathway in the mutants. Further research expanding on this observation will be important to understand the adipose phenotype of our *fstl1a* mutant line since it has been shown that *Shh* signalling can inhibit preadipocyte differentiation [68,71,72] but also the commitment of mesenchymal stem cells into the adipogenic lineage [47,48,73]. Also, *Fstl1* has been shown to regulate bone morphogenetic protein 4 (BMP4) signalling [57,61], a pro-adipogenic pathway required both for differentiation of preadipocytes and the commitment of mesenchymal stem cells to the adipose line [74–76]. Interestingly, reports show evidence of cilia modulating BMP4 signalling and, BMP4 regulating cilia at least in some cell types [77,78]. It will be interesting to direct future work to test whether there is a link between FSTL1, cilia, BMP signalling, and adipose tissue.

Finally, unlike murine models, our zebrafish line is a whole-body mutant, and adults are viable. Therefore, we have generated a reagent that could be used to study the function of *fstl1a* in other biological processes. For example, one question is whether *fstl1a* could contribute to adipose tissue expansion through its action over different cell types. For example, several reports support a role for FSTL1 in endothelial cells and angiogenesis [64,79,80] that is potentially relevant to our research given the intimate relationship between adipose tissue vasculature and preadipocytes, adipogenesis and overall tissue functionality as a critical factor for healthy adipose tissue expansion [81–84].

Dissecting the exact biological role of FSTL1 in adipose tissue will be important to understand obesity in BBS. We have previously shown that *BBS4* regulates

FSTL1 levels affecting both its expression and secretion [30]. Thus, FSTL1 would be expected to be downregulated in a *BBS4* mutant background. Based on the data presented here, *BBS4* mutants could be expected to have impaired adipogenesis/adipose tissue development. However, knockdown of *Bbs4* in 3T3-F422A cells promotes proliferation and triglyceride accumulation [32], and *Bbs4* knockout mice recapitulate the obese phenotype of patients with mutations in BBS genes, including *BBS4* [20,22]. Therefore, these sets of results are not contradictory but rather likely reflect the complex regulation of adipogenesis. For example, our work in cells showed that high levels of *Fstl1* are required at the onset of differentiation but interestingly, downregulation of *Fstl1* once differentiation is ongoing is also required during adipogenesis [30]. Based on that, the outcome will likely depend on the extent of *Fstl1* impairment. The absence of *Fstl1* would initially impair differentiation, a possibility supported by the results presented here. Interestingly, in a *BBS4* mutant background, reduced *Fstl1* levels could be sufficient to allow for adipogenesis to initiate and even facilitate it at later stages, an intriguing possibility that will need to be tested. In sum, fully understanding the role of FSTL1 will likely provide important insight into the physiology of adipose tissue, information that will be relevant to understand BBS and non-syndromic obesity.

Methods

Zebrafish husbandry

Adult zebrafish (*Danio rerio*) were maintained and bred in a stand-alone system (Tecniplast), with controlled temperature (28°C), conductivity (700 $\mu\text{S}/\text{cm}^2$) and pH (7.5). They were fed once a day with 48-hour post hatching *Artemia salina* and twice a day with pellets (TetraMin) according to standard procedures [85]. We used the wild-type line TAB5, and the transgenic line used in this work was generated in this background (see below). Embryos were raised in system water, typically at 28.5°C, except for those to be analysed at 12 somite stage, which were maintained at 28.5°C for 4 hours and then switched to 24°C. Staging of embryos was performed according to Kimmel and collaborators [86], while larvae were staged according to Parichy and collaborators [44]. ARRIVE guidelines were followed.

Ethical approval

All the manipulations followed the approved animal care protocols (number 010–19 and 011–19) by the

‘Comité de Ética en el Uso de Animales’ (CEUA-Institut Pasteur de Montevideo), and local regulations by the ‘Comisión Nacional de Experimentación Animal’ (CNEA).

Larvae breeding and diets

Embryos were raised at 28°C in 100 mm Petri dishes (50 embryos/plate) in aquarium water with methylene blue until 5 dpf. Between 5 and 9 dpf, 100 larvae (approximately) were transferred to containers at room temperature with daily aquarium water changes. They were fed with Larval AP100 #1 (0.1 g/100 larvae, Zeigler) twice a day and 24-hour post hatching *Artemia* once a day. From 9 to 15 dpf, larvae were separated in groups of 60 individuals, transferred to the standalone system in 5 L tanks, and fed with a mixture of Larval AP100 #1 (0.1 g/100 larvae) and 100–200 µm Golden Pearls (Brine Shrimp Direct) (0.04 g/100 larvae) twice a day and once with 24 h *Artemia*. Then, larvae were separated into two experimental groups (standard – STD – and high fat diet –HFD) of 30 per 5 L tank. Both groups were fed with Larval AP100 #1 (0.1 g each/100 larvae) plus 100–200 µm Golden Pearls (0.1 g/100 larvae) twice a day and once with 24 h *Artemia*. Larvae in the HFD group had a daily supplement of chicken egg yolk (0.3 g/100 larvae; E0625, Sigma-Aldrich) outside the system for 1 hour. Regarding the dry food, the STD group had an input of 0.62 kcal/100 larvae with 29% in the form of fat, while the HFD group had an input of 1.66 kcal/100 larvae with 61.7% coming from fat. The number of larvae per group was decided based on the results of preliminary experiments, considering optimal growth, possible death of larvae that usually occurs in this period, and the variability of the response variable. While randomization was not possible due to the inability to mark individual larvae, we took special care to generate STD and HFD groups with the same SL distribution at 15 dpf. At this stage, sex is still not defined; thus, it could not be taken into consideration in the experimental design. Additionally, all groups were allocated in the same standalone system. LG, IS and PL were aware of group allocation at all stages.

Morpholino knockdowns

We designed two splice-blocking morpholinos targeting exon 2-intron 2 junction of *fstl1a* or *fstl1b* mRNAs: MO*fstl1a*, ACTTTCTGTCTTACCTCTGCATAGC; MO*fstl1b*, GGTTTGGTGTAACCTTACCTCGGCAT. Control injections were performed using a standard MO: ctrl-MO, CCTCTTACCTCAGTTACAATTTATA. All morpholinos were acquired from Gene Tools

(Philomath, USA). In all cases, MOs were injected into the yolk of 1–4 cell-stage embryos from the same clutch of eggs, at the indicated doses in a maximum volume of 4 nl. To assess the efficiency of knockdown, total RNA was extracted from pooled morphant or wild-type embryos (~30) at 48 hpf using TRIzol reagent (Invitrogen), and cDNA was prepared using random hexamers and the SuperScript II First-Strand Synthesis System (Thermo). Then, a semi-quantitative PCR with primers flanking the morpholino targeting sites and GAPDH as control was used to evaluate knockdowns (Table S1).

CRISPR/Cas9 mutagenesis

Using the CRISPR Scan tool, two RNA guides were designed against exon 3 of *fstl1a* and four RNA guides against different exons of *fstl1b* (Table S1) and synthesized *in vitro* as described previously [42]. Briefly, the target-specific oligos were annealed with the tail oligo (Table S1), the product was amplified by PCR, column-purified and used as template for *in vitro* transcription with T7 RNA polymerase (*Maxi Script Ambion*). The resulting gRNAs were purified by precipitation with sodium acetate and ethanol or using the Monarch RNA Cleanup Kit (NEB) [87].

Cas9 or Cas9-nanos mRNA was synthesized *in vitro* using T3 (*mMESSAGE mMACHINE Transcription Kit*, Thermo) and purified using the *RNeasy Mini Kit* (Qiagen). Cas9 protein (Alt-R™ S.p. HiFi Cas9 Nuclease V3) was obtained from IDT. 200 pg of Cas9 or Cas9-nanos mRNA were mixed with 50 pg of gRNA and injected into the cytoplasm of one-cell stage embryos. For Crispr in F0, 1.25 µM Cas9 protein was incubated with 62.5 ng/µl of total gRNA and injected into the yolk of one-cell stage embryos.

The efficacy of our approach to generate mutations in *fstl1a* was evaluated in Cas9 plus gRNA-injected embryos through PCR with primers flanking exon 3 of *fstl1a* (Table S1) and agarose gel electrophoresis. We injected Cas9-nanos mRNA plus gRNA*fstl1a_1* to generate the stable line and bred the embryos. Once sexually mature, we screened for mutations through PCR of exon 3 and sequencing (Table S1). The selected fish was outcrossed with TAB5 to reduce the potential effect of off-target mutations. Genotyping of the mutation selected in this study was done using allele-specific primers (Table S1).

Whole-mount immunofluorescence and confocal microscopy

For immunofluorescence of whole embryos, we processed samples as reported previously [88], using the

following antibodies and stains that have been extensively used for visualizing cilia and actin in zebrafish [89]: anti-acetylated tubulin (1/750; T7451, Sigma); anti-mouse-488 (1/1000; A21202, Thermo); phalloidin-TMRM (1/8000; P1951, Sigma) in 48 hpf embryos and anti-acetylated tubulin (1/750; T7451, Sigma); anti-mouse IgG2b-568 (1/1000; A21144, Thermo) in Kupffer's vesicle. Confocal imaging of whole-mount embryos was performed using a Zeiss LSM880 microscope with an LD ICI Plan-Apochromat 25×/0.4 DIC M27 objective, using glycerol immersion. Images were analysed using Fiji [90]. Primary cilia lengths in Kupffer's vesicles were measured manually using the freehand-line tool in maximum intensity z-projections of the confocal stacks.

Analysis of adipose tissue extension

Lipid staining was performed as described previously [43]. Briefly, 12-hour fasted larvae were incubated for 1 hour in 100 mm Petri dishes with a Nile Red (Sigma-Aldrich, N1142) solution (0.25 µg/ml in aquarium water). To obtain the images, larvae were anesthetized in 0.04 g/l MS222 (Sigma-Aldrich, A5040), then incubated in 10 mg/ml epinephrine (Sigma-Aldrich, E4375) plus 0.06 g/l MS222 solution for 5 min to contract melanosomes, and mounted on 3% methylcellulose (Sigma-Aldrich, MO387). We acquired bright field and fluorescence images from the right side of each larva using a Canon EOS Rebel T3i camera associated with a Nikon SMZ 800 stereomicroscope equipped with a Mercury UV lamp. The staging of larvae was carried out by measuring their standard length (SL [44]: the distance from the snout to the caudal peduncle in brightfield images), using the line tool in Fiji. The visceral adipose tissue extension was quantified by making a mask using the threshold tool in Fiji.

qPCR

To quantify the relative expression of different molecular markers, after image acquisition, the abdominal region or visceral adipose tissue of each larva was dissected, placed in TRIzol reagent (Thermo) and stored at -80°C until the extraction of RNA using the protocol provided by the manufacturer. cDNA was synthesized using the SuperScript II First-Strand Synthesis System (Thermo) with oligo dT. qPCR was performed in Quant Studio 3 equipment (Thermo) with KAPA SYBR® FAST Kit (Sigma, KK4600). The primers used for each gene are listed in Table S1. The normalized relative quantity (NRQ) was calculated

following the protocol described in [91] with the mean group amplification efficiencies extracted using LinRegPCR software (v 2021.2) [92]. *ef1a* and *rpl13a* were used as housekeeping genes [93–95].

Statistical analysis

The statistical analysis was performed using Past software [96], GraphPad-Prism or R. Normality and homoscedasticity were checked using Shapiro–Wilk and Levene or F-test, respectively. The tests used for comparison of data sets are indicated in each case. Significant differences were considered when the p-value was less than 0.05.

Acknowledgments

We thank all members of the Human Molecular Genetics Lab and the Zebrafish Lab at the Institut Pasteur de Montevideo for their help along this work and critical reading of the manuscript. The authors gratefully acknowledge the Advanced Bioimaging Unit at the Institut Pasteur Montevideo for their support and assistance in the present work.

Disclosure statement

No potential conflict of interest was reported by the author(s).

Funding

This study was supported by Programa para el Desarrollo de las Ciencias Básicas (PEDECIBA) and Sistema Nacional de Investigadores- Agencia Nacional de Investigación e Innovación (ANII) to LG, IS, MC-R, HN, VP-E, PL and JLB; FCE_1_2019_1_156365 ANII to PL and JLB; Comisión Académica de Posgrados (CAP-UdelaR) to IS; FOCES – Fondo para la Convergencia Estructural del Mercosur (COF 03/11). The funders had no role in study design, data collection and analysis, decision to publish, or preparation of the manuscript.

Author contribution

LG, ISR, MCR, MA, GG, VPE, PL: experimental design and performed the experiments. Reviewed the manuscript. HN: statistical analysis of the data. Reviewed the manuscript. PL and JLB: funding acquisition, coordinated the project, coordinated experimental design, reviewed and edited the manuscript. LG, PL and JLB wrote the original manuscript. All authors have read and approved the final version of the manuscript.

Data availability statement

The data that support the findings of this study will be openly available in Figshare at doi: 10.6084/m9.figshare.26950657.

ORCID

Jose L. Badano  <http://orcid.org/0000-0002-0706-8652>

References

- [1] Bluher M. Obesity: global epidemiology and pathogenesis. *Nat Rev Endocrinol.* 2019;15(5):288–298. doi: [10.1038/s41574-019-0176-8](https://doi.org/10.1038/s41574-019-0176-8) PubMed PMID: 30814686.
- [2] Singh RK, Kumar P, Mahalingam K. Molecular genetics of human obesity: a comprehensive review. *C R Biol.* 2017;340(2):87–108. doi: [10.1016/j.crvi.2016.11.007](https://doi.org/10.1016/j.crvi.2016.11.007) Epub 20170113. PubMed PMID: 28089486.
- [3] Badano JL, Mitsuma N, Beales PL, et al. The ciliopathies: an emerging class of human genetic disorders. *Annu Rev Genom Hum Genet.* 2006;7(1):125–148. doi: [10.1146/annurev.genom.7.080505.115610](https://doi.org/10.1146/annurev.genom.7.080505.115610)
- [4] Fliegauf M, Benzing T, Omran H. When cilia go bad: cilia defects and ciliopathies. *Nat Rev Mol Cell Biol.* 2007;8(11):880–893. doi: [10.1038/nrm2278](https://doi.org/10.1038/nrm2278)
- [5] Hildebrandt F, Benzing T, Katsanis N. Ciliopathies. *N Engl J Med.* 2011;364(16):1533–1543. doi: [10.1056/NEJMra1010172](https://doi.org/10.1056/NEJMra1010172) PubMed PMID: 21506742; PubMed Central PMCID: PMC3640822.
- [6] Reiter JF, Leroux MR. Genes and molecular pathways underpinning ciliopathies. *Nat Rev Mol Cell Biol.* 2017;18(9):533–547. doi: [10.1038/nrm.2017.60](https://doi.org/10.1038/nrm.2017.60) Epub 20170712. PubMed PMID: 28698599; PubMed Central PMCID: PMC5851292.
- [7] Cardenas-Rodriguez M, Badano JL. Ciliary biology: understanding the cellular and genetic basis of human ciliopathies. *Am J Med Genet Part C Semin Med Genet.* 2009;151C(4):263–280. doi: [10.1002/ajmg.c.30227](https://doi.org/10.1002/ajmg.c.30227)
- [8] Nishimura Y, Kasahara K, Shiromizu T, et al. Primary cilia as signaling hubs in health and disease. *Adv Sci (Weinh).* 2019;6(1):1801138. doi: [10.1002/adv.201801138](https://doi.org/10.1002/adv.201801138) Epub 20181116. PubMed PMID: 30643718; PubMed Central PMCID: PMC6325590.
- [9] Mill P, Christensen ST, Pedersen LB. Primary cilia as dynamic and diverse signalling hubs in development and disease. *Nat Rev Genet.* 2023;24(7):421–441. doi: [10.1038/s41576-023-00587-9](https://doi.org/10.1038/s41576-023-00587-9) Epub 20230418. PubMed PMID: 37072495; PubMed Central PMCID: PMC67615029.
- [10] Yanardag S, Pugacheva EN. Primary cilium is involved in stem cell differentiation and renewal through the regulation of multiple signaling pathways. *Cells.* 2021;10(6): 1428. doi: [10.3390/cells10061428](https://doi.org/10.3390/cells10061428) Epub 20210608. PubMed PMID: 34201019; PubMed Central PMCID: PMC8226522.
- [11] Engle SE, Bansal R, Antonellis PJ, et al. Cilia signaling and obesity. *Semin Cell Dev Biol.* 2021;110:43–50. doi: [10.1016/j.semcdb.2020.05.006](https://doi.org/10.1016/j.semcdb.2020.05.006) Epub 20200525. PubMed PMID: 32466971; PubMed Central PMCID: PMC68739279.
- [12] Novas R, Cardenas-Rodriguez M, Irigoien F, et al. Bardet-biedl syndrome: Is it only cilia dysfunction? *FEBS Lett.* 2015;589(22):3479–3491. doi: [10.1016/j.febslet.2015.07.031](https://doi.org/10.1016/j.febslet.2015.07.031) PubMed PMID: 26231314.
- [13] Berbari NF, Lewis JS, Bishop GA, et al. Bardet–biedl syndrome proteins are required for the localization of G protein-coupled receptors to primary cilia. *Proc Natl Acad Sci USA.* 2008;105(11):4242–4246. doi: [10.1073/pnas.0711027105](https://doi.org/10.1073/pnas.0711027105)
- [14] Guo DF, Lin Z, Wu Y, et al. The BBSome in POMC and AgRP neurons is necessary for body weight regulation and sorting of metabolic receptors. *Diabetes.* 2019;68(8):1591–1603. doi: [10.2337/db18-1088](https://doi.org/10.2337/db18-1088) Epub 20190524. PubMed PMID: 31127052; PubMed Central PMCID: PMC6692817.
- [15] Loktev AV, Jackson PK. Neuropeptide Y family receptors traffic via the Bardet-Biedl syndrome pathway to signal in neuronal primary cilia. *Cell Rep.* 2013;5(5):1316–1329. doi: [10.1016/j.celrep.2013.11.011](https://doi.org/10.1016/j.celrep.2013.11.011) Epub 2013/12/10. PubMed PMID: 24316073.
- [16] Seo S, Guo DF, Bugge K, et al. Requirement of Bardet-Biedl syndrome proteins for leptin receptor signaling. *Hum Mol Genet.* 2009;18(7):1323–1331. doi: [10.1093/hmg/ddp031](https://doi.org/10.1093/hmg/ddp031) PubMed PMID: 19150989; PubMed Central PMCID: PMC2655773.
- [17] Guo DF, Cui H, Zhang Q, et al. The BBSome controls energy homeostasis by mediating the transport of the leptin receptor to the plasma membrane. *PLoS Genet.* 2016;12(2):e1005890. doi: [10.1371/journal.pgen.1005890](https://doi.org/10.1371/journal.pgen.1005890) PubMed PMID: 26926121; PubMed Central PMCID: PMC4771807.
- [18] Guo DF, Williams PA, Laule C, et al. POMC neuron BBSome regulation of body weight is independent of its ciliary function. *Function (Oxf).* 2024;5(1):zqad070. doi: [10.1093/function/zqad070](https://doi.org/10.1093/function/zqad070) Epub 20231223. PubMed PMID: 38223458; PubMed Central PMCID: PMC67615029.
- [19] Davis RE, Swiderski RE, Rahmouni K, et al. A knockin mouse model of the Bardet-Biedl syndrome 1 M390R mutation has cilia defects, ventriculomegaly, retinopathy, and obesity. *Proc Natl Acad Sci USA.* 2007;104(49):19422–19427. doi: [10.1073/pnas.0708571104](https://doi.org/10.1073/pnas.0708571104) PubMed PMID: 18032602; PubMed Central PMCID: PMC2148305.
- [20] Eichers ER, Abd-El-Barr MM, Paylor R, et al. Phenotypic characterization of Bbs4 null mice reveals age-dependent penetrance and variable expressivity. *Hum Genet.* 2006;120(2):211–226. doi: [10.1007/s00439-006-0197-y](https://doi.org/10.1007/s00439-006-0197-y) PubMed PMID: 16794820.
- [21] Fath MA, Mullins RF, Searby C, et al. Mkks-null mice have a phenotype resembling Bardet–Biedl syndrome. *Hum Mol Genet.* 2005;14(9):1109–1118. doi: [10.1093/hmg/ddi123](https://doi.org/10.1093/hmg/ddi123)
- [22] Mykytyn K, Mullins RF, Andrews M, et al. Bardet-Biedl syndrome type 4 (BBS4)-null mice implicate Bbs4 in flagella formation but not global cilia assembly. *Proc Natl Acad Sci USA.* 2004;101(23):8664–8669. doi: [10.1073/pnas.0402354101](https://doi.org/10.1073/pnas.0402354101) Epub 2004/06/03. PubMed PMID: 15173597; PubMed Central PMCID: PMC423252.
- [23] Nishimura DY, Fath M, Mullins RF, et al. Bbs2-null mice have neurosensory deficits, a defect in social dominance, and retinopathy associated with mislocalization of rhodopsin. *Proc Natl Acad Sci USA.* 2004;101(47):16588–16593. doi: [10.1073/pnas.0405496101](https://doi.org/10.1073/pnas.0405496101)

- [24] Rouabhi M, Guo DF, Morgan DA, et al. Bbsome ablation in SF1 neurons causes obesity without comorbidities. *Mol Metab.* 2021;48:101211. doi: [10.1016/j.molmet.2021.101211](https://doi.org/10.1016/j.molmet.2021.101211) Epub 20210313. PubMed PMID: 33722691; PubMed Central PMCID: PMCPCMC8065214.
- [25] Hilgendorf KI. Primary cilia are critical regulators of white adipose tissue expansion. *Front Physiol.* 2021;12:769367. Epub 20211025. doi: [10.3389/fphys.2021.769367](https://doi.org/10.3389/fphys.2021.769367) PubMed PMID: 34759842; PubMed Central PMCID: PMCPCMC8573240.
- [26] Tummala P, Arnsdorf EJ, Jacobs CR. The role of primary cilia in mesenchymal stem cell differentiation: a pivotal switch in guiding lineage commitment. *Cell Mol Bioeng.* 2010;3(3):207–212. doi: [10.1007/s12195-010-0127-x](https://doi.org/10.1007/s12195-010-0127-x) PubMed PMID: 20823950; PubMed Central PMCID: PMC2930791.
- [27] Forcioli-Conti N, Lacas-Gervais S, Dani C, et al. The primary cilium undergoes dynamic size modifications during adipocyte differentiation of human adipose stem cells. *Biochem Biophys Res Commun.* 2015;458(1):117–122. doi: [10.1016/j.bbrc.2015.01.078](https://doi.org/10.1016/j.bbrc.2015.01.078) PubMed PMID: 25637533.
- [28] Hilgendorf KI, Johnson CT, Mezger A, et al. Omega-3 fatty acids activate ciliary FFAR4 to control adipogenesis. *Cell.* 2019;179(6):1289–305 e21. Epub 20191121. doi: [10.1016/j.cell.2019.11.005](https://doi.org/10.1016/j.cell.2019.11.005) PubMed PMID: 31761534; PubMed Central PMCID: PMCPCMC7332222.
- [29] Marion V, Stoetzel C, Schlicht D, et al. Transient ciliogenesis involving Bardet-Biedl syndrome proteins is a fundamental characteristic of adipogenic differentiation. *Proc Natl Acad Sci USA.* 2009;106(6):1820–1825. doi: [10.1073/pnas.0812518106](https://doi.org/10.1073/pnas.0812518106)
- [30] Prieto-Echagüe V, Lodh S, Colman L, et al. BBS4 regulates the expression and secretion of FSTL1, a protein that participates in ciliogenesis and the differentiation of 3T3-L1. *Sci Rep.* 2017;7(1). doi: [10.1038/s41598-017-10330-0](https://doi.org/10.1038/s41598-017-10330-0)
- [31] Forti E, Aksanov O, Birk RZ. Temporal expression pattern of Bardet-Biedl syndrome genes in adipogenesis. *Int J Biochem Cell Biol.* 2007;39(5):1055–1062. doi: [10.1016/j.biocel.2007.02.014](https://doi.org/10.1016/j.biocel.2007.02.014) PubMed PMID: 17379567.
- [32] Aksanov O, Green P, Birk RZ. BBS4 directly affects proliferation and differentiation of adipocytes. *Cell Mol Life Sci.* 2014;71(17):3381–3392. doi: [10.1007/s00018-014-1571-x](https://doi.org/10.1007/s00018-014-1571-x) PubMed PMID: 24500759.
- [33] Marion V, Mockel A, De Melo C, et al. Bbs-induced ciliary defect enhances adipogenesis, causing paradoxical higher-insulin sensitivity, glucose usage, and decreased inflammatory response. *Cell Metab.* 2012;16(3):363–377. doi: [10.1016/j.cmet.2012.08.005](https://doi.org/10.1016/j.cmet.2012.08.005) PubMed PMID: 22958920.
- [34] Mattiotti A, Prakash S, Barnett P, et al. Follistatin-like 1 in development and human diseases. *Cell Mol Life Sci.* 2018;75(13):2339–2354. doi: [10.1007/s00018-018-2805-0](https://doi.org/10.1007/s00018-018-2805-0) Epub 2018/03/30. PubMed PMID: 29594389; PubMed Central PMCID: PMCPCMC5986856.
- [35] Wu Y, Zhou S, Smas CM. Downregulated expression of the secreted glycoprotein follistatin-like 1 (Fstl1) is a robust hallmark of preadipocyte to adipocyte conversion. *Mech Dev.* 2010;127(3–4):183–202. doi: [10.1016/j.mod.2009.12.003](https://doi.org/10.1016/j.mod.2009.12.003) PubMed PMID: 20043993; PubMed Central PMCID: PMC2849861.
- [36] Fang D, Shi X, Jia X, et al. Ups and downs: the PPARgamma/p-PPARgamma seesaw of follistatin-like 1 and integrin receptor signaling in adipogenesis. *Mol Metab.* 2022;55:101400. doi: [10.1016/j.molmet.2021.101400](https://doi.org/10.1016/j.molmet.2021.101400) Epub 20211120. PubMed PMID: 34813964; PubMed Central PMCID: PMCPCMC8683615.
- [37] Liu X, Liu Y, Li X, et al. Follistatin like-1 (Fstl1) is required for the normal formation of lung airway and vascular smooth muscle at birth. *PLoS One.* 2017;12(6):e0177899. doi: [10.1371/journal.pone.0177899](https://doi.org/10.1371/journal.pone.0177899) Epub 2017/06/03. PubMed PMID: 28574994; PubMed Central PMCID: PMCPCMC5456059.
- [38] Li X, Li L, Chang Y, et al. Structural and functional study of FK domain of Fstl1. *Protein Sci.* 2019;28(10):1819–1829. doi: [10.1002/pro.3696](https://doi.org/10.1002/pro.3696) PubMed PMID: 31351024; PubMed Central PMCID: PMCPCMC6739823. Epub 20190809.
- [39] Dal-Pra S, Furthauer M, Van-Celst J, et al. Noggin1 and follistatin-like2 function redundantly to chordin to antagonize BMP activity. *Dev Biol.* 2006;298(2):514–526. doi: [10.1016/j.ydbio.2006.07.002](https://doi.org/10.1016/j.ydbio.2006.07.002) Epub 20060712. PubMed PMID: 16890217.
- [40] Esterberg R, Delalande JM, Fritz A. Tailbud-derived Bmp4 drives proliferation and inhibits maturation of zebrafish chordamesoderm. *Development.* 2008;135(23):3891–3901. doi: [10.1242/dev.029264](https://doi.org/10.1242/dev.029264) Epub 2008/10/25. PubMed PMID: 18948415; PubMed Central PMCID: PMCPCMC2765817.
- [41] Essner JJ, Amack JD, Nyholm MK, et al. Kupffer's vesicle is a ciliated organ of asymmetry in the zebrafish embryo that initiates left-right development of the brain, heart and gut. *Development.* 2005;132(6):1247–1260. doi: [10.1242/dev.01663](https://doi.org/10.1242/dev.01663)
- [42] Moreno-Mateos MA, Vejnar CE, Beaudoin JD, et al. Crisprscan: designing highly efficient sgRNAs for CRISPR-Cas9 targeting in vivo. *Nat Methods.* 2015;12(10):982–988. doi: [10.1038/nmeth.3543](https://doi.org/10.1038/nmeth.3543) PubMed PMID: 26322839; PubMed Central PMCID: PMCPCMC4589495.
- [43] Minchin JE, Rawls JF. In vivo imaging and quantification of regional adiposity in zebrafish. *Methods Cell Biol.* 2017;138:3–27. doi: [10.1016/bs.mcb.2016.11.010](https://doi.org/10.1016/bs.mcb.2016.11.010) Epub 2017/01/29. PubMed PMID: 28129849; PubMed Central PMCID: PMCPCMC5497849.
- [44] Parichy DM, Elizondo MR, Mills MG, et al. Normal table of postembryonic zebrafish development: staging by externally visible anatomy of the living fish. *Dev Dyn.* 2009;238(12):2975–3015. doi: [10.1002/dvdy.22113](https://doi.org/10.1002/dvdy.22113) PubMed PMID: 19891001; PubMed Central PMCID: PMCPCMC3030279.
- [45] Minchin JEN, Rawls JF. A classification system for zebrafish adipose tissues. *Dis Model Mech.* 2017;10(6):797–809. doi: [10.1242/dmm.025759](https://doi.org/10.1242/dmm.025759) Epub 20170327. PubMed PMID: 28348140; PubMed Central PMCID: PMCPCMC5482999.
- [46] Wu RS, Lam II, Clay H, et al. A rapid method for directed gene knockout for screening in G0 zebrafish. *Dev Cell.* 2018;46(1):112–25 e4. doi: [10.1016/j.devcel.2018.06.003](https://doi.org/10.1016/j.devcel.2018.06.003) Epub 2018/07/06. PubMed PMID: 29974860.

- [47] James AW, Leucht P, Levi B, et al. Sonic hedgehog influences the balance of osteogenesis and adipogenesis in mouse adipose-derived stromal cells. *Tissue Eng Part A*. 2010;16(8):2605–2616. doi: [10.1089/ten.TEA.2010.0048](https://doi.org/10.1089/ten.TEA.2010.0048) PubMed PMID: 20367246; PubMed Central PMCID: PMCPMC2947454.
- [48] Spinella-Jaegle S, Rawadi G, Kawai S, et al. Sonic hedgehog increases the commitment of pluripotent mesenchymal cells into the osteoblastic lineage and abolishes adipocytic differentiation. *J Cell Sci*. 2001;Pt 114(11):2085–2094. doi: [10.1242/jcs.114.11.2085](https://doi.org/10.1242/jcs.114.11.2085) PubMed PMID: 11493644
- [49] Gerdes JM, Christou-Savina S, Xiong Y, et al. Ciliary dysfunction impairs beta-cell insulin secretion and promotes development of type 2 diabetes in rodents. *Nat Commun*. 2014;5(1):5308. doi: [10.1038/ncomms6308](https://doi.org/10.1038/ncomms6308) PubMed PMID: 25374274.
- [50] Lodh S, Hosteley TL, Leitch CC, et al. Differential effects on beta-cell mass by disruption of Bardet-Biedl syndrome or alstrom syndrome genes. *Hum Mol Genet*. 2016;25(1):57–68. doi: [10.1093/hmg/ddv447](https://doi.org/10.1093/hmg/ddv447) PubMed PMID: 26494903; PubMed Central PMCID: PMCPMC4690491.
- [51] Liu H, Wen J, Tian X, et al. miR-125a-3p regulates the expression of FSTL1, a pro-inflammatory factor, during adipogenic differentiation, and inhibits adipogenesis in mice. *Faseb J*. 2023;37(9):e23146. doi: [10.1096/fj.202300851R](https://doi.org/10.1096/fj.202300851R) PubMed PMID: 37584664.
- [52] El-Brolosy MA, Kontarakis Z, Rossi A, et al. Genetic compensation triggered by mutant mRNA degradation. *Nature*. 2019;568(7751):193–197. doi: [10.1038/s41586-019-1064-z](https://doi.org/10.1038/s41586-019-1064-z) Epub 2019/04/05. PubMed PMID: 30944477; PubMed Central PMCID: PMCPMC6707827.
- [53] El-Brolosy MA, Stainier DYR. Genetic compensation: a phenomenon in search of mechanisms. *PloS Genet*. 2017;13(7):e1006780. doi: [10.1371/journal.pgen.1006780](https://doi.org/10.1371/journal.pgen.1006780) Epub 2017/07/14. PubMed PMID: 28704371; PubMed Central PMCID: PMCPMC5509088.
- [54] Rossi A, Kontarakis Z, Gerri C, et al. Genetic compensation induced by deleterious mutations but not gene knockdowns. *Nature*. 2015;524(7564):230–233. doi: [10.1038/nature14580](https://doi.org/10.1038/nature14580) Epub 2015/07/15. PubMed PMID: 26168398.
- [55] Anderson JL, Mulligan TS, Shen MC, et al. mRNA processing in mutant zebrafish lines generated by chemical and crispr-mediated mutagenesis produces unexpected transcripts that escape nonsense-mediated decay. *PloS Genet*. 2017;13(11):e1007105. doi: [10.1371/journal.pgen.1007105](https://doi.org/10.1371/journal.pgen.1007105) Epub 2017/11/22. PubMed PMID: 29161261; PubMed Central PMCID: PMCPMC5716581.
- [56] Ma Z, Zhu P, Shi H, et al. Ptc-bearing mRNA elicits a genetic compensation response via Upf3a and COMPASS components. *Nature*. 2019;568(7751):259–263. doi: [10.1038/s41586-019-1057-y](https://doi.org/10.1038/s41586-019-1057-y) Epub 2019/04/05. PubMed PMID: 30944473.
- [57] Geng Y, Dong Y, Yu M, et al. Follistatin-like 1 (Fstl1) is a bone morphogenetic protein (BMP) 4 signaling antagonist in controlling mouse lung development. *Proc Natl Acad Sci USA*. 2011;108(17):7058–7063. doi: [10.1073/pnas.1007293108](https://doi.org/10.1073/pnas.1007293108) PubMed PMID: 21482757; PubMed Central PMCID: PMCPMC3084141.
- [58] Ouchi N, Asaumi Y, Ohashi K, et al. DIP2A functions as a FSTL1 receptor. *J Biol Chem*. 2010;285(10):7127–7134. doi: [10.1074/jbc.M109.069468](https://doi.org/10.1074/jbc.M109.069468) PubMed PMID: 20054002; PubMed Central PMCID: PMCPMC2844162.
- [59] Tanaka M, Murakami K, Ozaki S, et al. DIP2 interacting protein 2 homolog a (drosophila) is a candidate receptor for follistatin-related protein/follistatin-like 1—analysis of their binding with tgfbeta superfamily proteins. *FEBS J*. 2010;277(20):4278–4289. doi: [10.1111/j.1742-4658.2010.07816.x](https://doi.org/10.1111/j.1742-4658.2010.07816.x) PubMed PMID: 20860622.
- [60] Cardenas-Rodriguez M, Austin-Tse C, Bergboer JGM, et al. Genetic compensation for cilia defects in cep290 mutants by upregulation of cilia-associated small GTPases. *J Cell Sci*. 2021;134(14). doi: [10.1242/jcs.258568](https://doi.org/10.1242/jcs.258568) Epub 2021/06/23. PubMed PMID: 34155518; PubMed Central PMCID: PMCPMC8325957.
- [61] Sylva M, Li VS, Buffing AA, et al. The BMP antagonist follistatin-like 1 is required for skeletal and lung organogenesis. *PLOS ONE*. 2011;6(8):e22616. doi: [10.1371/journal.pone.0022616](https://doi.org/10.1371/journal.pone.0022616) PubMed PMID: 21826198; PubMed Central PMCID: PMCPMC3149603.
- [62] Rao J, Wang H, Ni M, et al. FSTL1 promotes liver fibrosis by reprogramming macrophage function through modulating the intracellular function of PKM2. *Gut*. 2022;71(12):2539–2550. doi: [10.1136/gutjnl-2021-325150](https://doi.org/10.1136/gutjnl-2021-325150) Epub 2022/02/09. PubMed PMID: 35140065; PubMed Central PMCID: PMCPMC9664121.
- [63] Shimano M, Ouchi N, Nakamura K, et al. Cardiac myocyte follistatin-like 1 functions to attenuate hypertrophy following pressure overload. *Proc Natl Acad Sci USA*. 2011;108(43):E899–906. doi: [10.1073/pnas.1108559108](https://doi.org/10.1073/pnas.1108559108) Epub 2011/10/10. PubMed PMID: 21987816; PubMed Central PMCID: PMCPMC3203781.
- [64] Tania NP, Maarsingh H, Is TB, et al. Endothelial follistatin-like-1 regulates the postnatal development of the pulmonary vasculature by modulating BMP/Smad signaling. *Pulm Circ*. 2017;7(1):219–231. doi: [10.1177/2045893217702340](https://doi.org/10.1177/2045893217702340) Epub 2017/03/15. PubMed PMID: 28680581; PubMed Central PMCID: PMCPMC5448549.
- [65] Flynn EJ 3rd, Trent CM, Rawls JF. Ontogeny and nutritional control of adipogenesis in zebrafish (*Danio rerio*). *J Lipid Res*. 2009;50(8):1641–1652. doi: [10.1194/jlr.M800590-JLR200](https://doi.org/10.1194/jlr.M800590-JLR200) Epub 2009/04/16. PubMed PMID: 19366995; PubMed Central PMCID: PMCPMC2724053.
- [66] Rouf MA, Wen L, Mahendra Y, et al. The recent advances and future perspectives of genetic compensation studies in the zebrafish model. *Genes Dis*. 2023;10(2):468–479. doi: [10.1016/j.gendis.2021.12.003](https://doi.org/10.1016/j.gendis.2021.12.003) Epub 2022/01/05. PubMed PMID: 37223518; PubMed Central PMCID: PMCPMC10201552.
- [67] Zhu D, Shi S, Wang H, et al. Growth arrest induces primary-cilium formation and sensitizes IGF-1-receptor signaling during differentiation induction of 3T3-L1 preadipocytes. *J Cell Sci*. 2009;122

- (15):2760–2768. doi: [10.1242/jcs.046276](https://doi.org/10.1242/jcs.046276) Epub 2009/07/15. PubMed PMID: 19596798.
- [68] Cousin W, Dani C, Peraldi P. Inhibition of the anti-adipogenic Hedgehog signaling pathway by cyclo-pamine does not trigger adipocyte differentiation. *Biochem Biophys Res Commun.* 2006;349(2):799–803. doi: [10.1016/j.bbrc.2006.08.112](https://doi.org/10.1016/j.bbrc.2006.08.112) PubMed PMID: 16949046.
- [69] Goetz SC, Anderson KV. The primary cilium: a signalling centre during vertebrate development. *Nat Rev Genet.* 2010;11(5):331–344. doi: [10.1038/nrg2774](https://doi.org/10.1038/nrg2774) PubMed PMID: 20395968; PubMed Central PMCID: PMC3121168.
- [70] Ross SE, Hemati N, Longo KA, et al. Inhibition of adipogenesis by Wnt signaling. *Science.* 2000;289(5481):950–953. doi: [10.1126/science.289.5481.950](https://doi.org/10.1126/science.289.5481.950) PubMed PMID: 10937998
- [71] Zehentner BK, Leser U, Burtscher H. BMP-2 and sonic hedgehog have contrary effects on adipocyte-like differentiation of C3H10T1/2 cells. *DNA Cell Biol.* 2000;19(5):275–281. doi: [10.1089/10445490050021186](https://doi.org/10.1089/10445490050021186) PubMed PMID: 10855794.
- [72] Mariman EC, Vink RG, Roumans NJ, et al. The cilium: a cellular antenna with an influence on obesity risk. *Br J Nutr.* 2016;116(4):576–592. doi: [10.1017/S0007114516002282](https://doi.org/10.1017/S0007114516002282) PubMed PMID: 27323230.
- [73] van der Horst G, Farih-Sips H, Lowik CW, et al. Hedgehog stimulates only osteoblastic differentiation of undifferentiated KS483 cells. *Bone.* 2003;33(6):899–910. doi: [10.1016/j.bone.2003.07.004](https://doi.org/10.1016/j.bone.2003.07.004) PubMed PMID: 14678849
- [74] Bowers RR, Kim JW, Otto TC, et al. Stable stem cell commitment to the adipocyte lineage by inhibition of DNA methylation: role of the BMP-4 gene. *Proc Natl Acad Sci USA.* 2006;103(35):13022–13027. doi: [10.1073/pnas.0605789103](https://doi.org/10.1073/pnas.0605789103) PubMed PMID: 16916928; PubMed Central PMCID: PMC1559746.
- [75] Huang H, Song TJ, Li X, et al. BMP signaling pathway is required for commitment of C3H10T1/2 pluripotent stem cells to the adipocyte lineage. *Proc Natl Acad Sci USA.* 2009;106(31):12670–12675. doi: [10.1073/pnas.0906266106](https://doi.org/10.1073/pnas.0906266106) PubMed PMID: 19620713; PubMed Central PMCID: PMC2722335.
- [76] Suenaga M, Kurosawa N, Asano H, et al. Bmp4 expressed in preadipocytes is required for the onset of adipocyte differentiation. *Cytokine.* 2013;64(1):138–145. doi: [10.1016/j.cyto.2013.07.011](https://doi.org/10.1016/j.cyto.2013.07.011) PubMed PMID: 23911203.
- [77] Hiraoka K, Inada H, Yanai K, et al. Bone morphogenetic proteins inhibit ciliogenesis of ependymal cells in vitro. *Tohoku J Exp Med.* 2020;252(3):199–208. doi: [10.1620/tjem.252.199](https://doi.org/10.1620/tjem.252.199) PubMed PMID: 33087680.
- [78] Willaredt MA, Gorgas K, Gardner HA, et al. Multiple essential roles for primary cilia in heart development. *Cilia.* 2012;1(1):23. doi: [10.1186/2046-2530-1-23](https://doi.org/10.1186/2046-2530-1-23) Epub 20121211. PubMed PMID: 23351706; PubMed Central PMCID: PMC3563622.
- [79] Lei ST, Li MQ, Cao YL, et al. Follistatin-like I promotes endometriosis by increasing proinflammatory factors and promoting angiogenesis. *Reproduction.* 2021;163(1):57–68. doi: [10.1530/REP-21-0094](https://doi.org/10.1530/REP-21-0094) Epub 20211230. PubMed PMID: 34866594.
- [80] Ouchi N, Oshima Y, Ohashi K, et al. Follistatin-like 1, a secreted muscle protein, promotes endothelial cell function and revascularization in ischemic tissue through a nitric-oxide synthase-dependent mechanism. *J Biol Chem.* 2008;283(47):32802–32811. doi: [10.1074/jbc.M803440200](https://doi.org/10.1074/jbc.M803440200) PubMed PMID: 18718903; PubMed Central PMCID: PMC2583310.
- [81] Cao Y. Angiogenesis modulates adipogenesis and obesity. *J Clin Invest.* 2007;117(9):2362–2368. doi: [10.1172/JCI32239](https://doi.org/10.1172/JCI32239) PubMed PMID: 17786229; PubMed Central PMCID: PMC1963348.
- [82] Crewe C, An YA, Scherer PE. The ominous triad of adipose tissue dysfunction: inflammation, fibrosis, and impaired angiogenesis. *J Clin Invest.* 2017;127(1):74–82. doi: [10.1172/JCI88883](https://doi.org/10.1172/JCI88883) Epub 20170103. PubMed PMID: 28045400; PubMed Central PMCID: PMC5199684.
- [83] Rudnicki M, Abdifarkosh G, Rezvan O, et al. Female mice have higher angiogenesis in perigonadal adipose tissue than males in response to high-fat diet. *Front Physiol.* 2018;9:1452. doi: [10.3389/fphys.2018.01452](https://doi.org/10.3389/fphys.2018.01452) Epub 20181023. PubMed PMID: 30405427; PubMed Central PMCID: PMC6206240.
- [84] Tang W, Zeve D, Suh JM, et al. White fat progenitor cells reside in the adipose vasculature. *Science.* 2008;322(5901):583–586. doi: [10.1126/science.1156232](https://doi.org/10.1126/science.1156232) Epub 20080918. PubMed PMID: 18801968; PubMed Central PMCID: PMC2597101.
- [85] Westerfield M. The zebrafish book. A guide for the laboratory use of zebrafish (*Danio rerio*). Eugene (OR): University of Oregon Press; 1995.
- [86] Kimmel CB, Ballard WW, Kimmel SR, et al. Stages of embryonic development of the zebrafish. *Dev Dyn.* 1995;203(3):253–310. doi: [10.1002/aja.1002030302](https://doi.org/10.1002/aja.1002030302) PubMed PMID: 8589427.
- [87] Varshney GK, Carrington B, Pei W, et al. A high-throughput functional genomics workflow based on CRISPR/Cas9-mediated targeted mutagenesis in zebrafish. *Nat Protoc.* 2016;11(12):2357–2375. doi: [10.1038/nprot.2016.141](https://doi.org/10.1038/nprot.2016.141) Epub 20161027. PubMed PMID: 27809318; PubMed Central PMCID: PMC5630457.
- [88] Lepanto P, Davison C, Casanova G, et al. Characterization of primary cilia during the differentiation of retinal ganglion cells in the zebrafish. *Neural Dev.* 2016;11(1):10. doi: [10.1186/s13064-016-0064-z](https://doi.org/10.1186/s13064-016-0064-z) PubMed PMID: 27053191; PubMed Central PMCID: PMC4823885.
- [89] Malicki J, Avanesov A, Li J, et al. Analysis of cilia structure and function in zebrafish. *Methods Cell Biol.* 2011;101:39–74. doi: [10.1016/B978-0-12-387036-0.00003-7](https://doi.org/10.1016/B978-0-12-387036-0.00003-7) PubMed PMID: 21550439.
- [90] Schindelin J, Arganda-Carreras I, Frise E, et al. Fiji: an open-source platform for biological-image analysis. *Nat Methods.* 2012;9(7):676–682. doi: [10.1038/nmeth.2019](https://doi.org/10.1038/nmeth.2019) PubMed PMID: 22743772; PubMed Central PMCID: PMC3855844.
- [91] Ganger MT, Dietz GD, Ewing SJ. A common base method for analysis of qPCR data and the application of simple blocking in qPCR experiments. *BMC Bioinformatics.* 2017;18(1):534. doi: [10.1186/s12859-](https://doi.org/10.1186/s12859-)

- 017-1949-5 Epub 20171201. PubMed PMID: 29191175; PubMed Central PMCID: PMC5709943.
- [92] Ruijter JM, Ramakers C, Hoogaars WM, et al. Amplification efficiency: linking baseline and bias in the analysis of quantitative PCR data. *Nucleic Acids Res.* 2009;37(6):e45. doi: [10.1093/nar/gkp045](https://doi.org/10.1093/nar/gkp045) Epub 20090222. PubMed PMID: 19237396; PubMed Central PMCID: PMC5709943.
- [93] Rassier GT, Silveira TLR, Remiao MH, et al. Evaluation of qPCR reference genes in gh-overexpressing transgenic zebrafish (*Danio rerio*). *Sci Rep.* 2020;10(1):12692. doi: [10.1038/s41598-020-69423-y](https://doi.org/10.1038/s41598-020-69423-y) Epub 20200729. PubMed PMID: 32728128; PubMed Central PMCID: PMC7391647.
- [94] Tang R, Dodd A, Lai D, et al. Validation of zebrafish (*Danio rerio*) reference genes for quantitative real-time RT-PCR normalization. *Acta Biochim Biophys Sin (Shanghai).* 2007;39(5):384–390. doi: [10.1111/j.1745-7270.2007.00283.x](https://doi.org/10.1111/j.1745-7270.2007.00283.x) PubMed PMID: 17492136; PubMed Central PMCID: PMC7110012.
- [95] Xu H, Li C, Zeng Q, et al. Genome-wide identification of suitable zebrafish *Danio rerio* reference genes for normalization of gene expression data by rt-qPCR. *J Fish Biol.* 2016;88(6):2095–2110. doi: [10.1111/jfb.12915](https://doi.org/10.1111/jfb.12915) Epub 20160428. PubMed PMID: 27126589.
- [96] Hammer Ø, Harper DAT, Ryan PD. PAST: paleontological statistics software package for education and data analysis. *Palaeontologia Electronica.* 2001;4(1):9.